

# Co-ligand dependent Formation and Phase Transformation of Four Porphyrin-based Cerium MOFs

*Timo Rhauderwiek,<sup>a</sup> Niclas Heidenreich,<sup>a,b</sup> Helge Reinsch,<sup>a</sup> Sigurd Øien-Ødegaard,<sup>c</sup> Kirill A. Lomachenko,<sup>d, e</sup> Uta Rütt,<sup>b</sup> Alexander V. Soldatov,<sup>d</sup> Karl Petter Lillerud,<sup>c</sup> Norbert Stock<sup>a,c,\*</sup>*

<sup>a</sup> Institut für Anorganische Chemie, Christian-Albrechts-Universität, Max-Eyth Straße 2,  
D-24118 Kiel, Germany

<sup>b</sup> Deutsches-Elektronen-Synchrotron DESY, Notkestraße 85, 22607 Hamburg

<sup>c</sup> Department of Chemistry, University of Oslo, Sem Sælands vei 26, N-0371 Oslo, Norway

<sup>d</sup> International Research Center “Smart Materials”, Southern Federal University, Zorge Street 5,  
344090 Rostov-on-Don, Russia

<sup>e</sup> European Synchrotron Radiation Facility, 71 avenue des Martyrs, CS 40220, 38043 Grenoble  
Cedex 9, France

KEYWORDS metal organic framework, in situ X-ray diffraction, cerium, porphyrin, phase transformation

**ABSTRACT:** The four porphyrin-based metal-organic frameworks (MOFs) containing  $\text{Ce}^{3+}$  ions,  $[\text{Ce}_4(\text{H}_2\text{TCPP})_3(\text{DMF})_2(\text{H}_2\text{O})_4]$  (**CAU-18**),  $[\text{Ce}_4(\text{H}_2\text{TCPP})_3] \cdot 22\text{H}_2\text{O}$  (**CAU-18a**),  $[\text{Ce}_3(\text{H}_2\text{TCPP})_2(\text{BA-X})(\text{HBA-X}/\text{H}_2\text{O})_2] \cdot 2 \text{HBA-X} \cdot n \text{H}_2\text{O}$  (**CAU-19-X** with  $\text{X}=\text{H}$ , 2Cl, 3Cl, 4Cl, 3CO<sub>2</sub>H, 4NH<sub>2</sub>, 4NO<sub>2</sub>,  $\text{HBA}=\text{C}_7\text{H}_4\text{O}_2$ ) and  $[\text{Ce}_2(\text{H}_2\text{TCPP})(\text{C}_7\text{H}_4\text{O}_2\text{NO}_2)_2] \cdot 2\text{DMF}$  (**Ce-PMOF-4NO<sub>2</sub>**) were synthesized using the linker 4-tetracarboxyphenylporphyrin ( $\text{H}_6\text{TCPP}$ ). The formation of the respective MOFs depends mainly on the presence of a co-ligand in the synthesis mixture. CAU-18 was obtained in the absence of a co-ligand while CAU-19-X was observed, when the benzoic acid derivative HBA-X ( $\text{X} = \text{H}$ , 2Cl, 3Cl, 4Cl, 3CO<sub>2</sub>H, 4NH<sub>2</sub>) was added. In case HBA-4NO<sub>2</sub> was used as a co-ligand, yet another compound Ce-PMOF-4NO<sub>2</sub> is obtained. The structures of CAU-18 and CAU-19-H were determined from single crystal X-ray diffraction data, while the structure of Ce-PMOF-4NO<sub>2</sub> was refined from PXRD data by the Rietveld method. Activation of CAU-18 and Ce-PMOF-4NO<sub>2</sub> resulted in phase transformations. Thermal treatment of CAU-18 at 250 °C leads to CAU-18a, which is porous towards N<sub>2</sub> and H<sub>2</sub>O, while treatment of Ce-PMOF-4NO<sub>2</sub> in organic solvents at 70 °C leads to the formation of CAU-19-4NO<sub>2</sub>, which cannot be synthesized directly. All CAU-19-X compounds are porous towards N<sub>2</sub> and H<sub>2</sub>O and the specific surface areas vary between 330 and 600 m<sup>2</sup> g<sup>-1</sup> depending on the size of the incorporated co-ligand. CAU-18, CAU-18a and CAU-19-X are thermally stable in air up to 330 °C and chemically stable in H<sub>2</sub>O and all tested organic solvents. Ce L<sub>3</sub>-edge XANES measurements revealed that exclusively  $\text{Ce}^{3+}$  ions are present in the title compounds, despite the use of  $(\text{NH}_4)_2[\text{Ce}(\text{NO}_3)_6]$  in all syntheses. In addition, the crystallization of CAU-18 and CAU-19-H was investigated *in situ* by synchrotron PXRD at DESY, Hamburg, using reaction temperatures between 110 and 130 °C. The data was evaluated using the approach by Gualtieri to determine the probability of nucleation ( $P_n$ ) and the Arrhenius activation energy

for nucleation ( $k_n$ ) and crystal growth ( $k_g$ ). The Arrhenius activation energies for the nucleation were determined as 47(2) and 56(3) kJ mol<sup>-1</sup> and for crystal growth 45(4) and 58(5) kJ mol<sup>-1</sup> for CAU-18 and CAU-19-H, respectively. The induction time ( $t_{ind}$ ), in which no crystalline products are detected and the total reaction time to achieve full conversion ( $t_{com}$ ) are shortened at higher temperatures. Furthermore the maximum of the probability of nucleation is shifted to earlier reaction times with increasing temperature.

## Introduction

The modular structure of metal organic frameworks (MOFs) allows one to tune the pore size and pore surface properties, which in turn leads to a large range of chemical and physical properties.<sup>1-4</sup> Hence MOFs have been investigated in applications such as gas storage and separation, drug delivery or catalysis.<sup>1,3,5-7</sup> *In situ* crystallization investigations were performed in recent years to study crystallization processes of MOFs in solution and to determine kinetic parameters. Examples comprise the formation of MIL-53<sup>8</sup> and MIL-100,<sup>9</sup> which are formed through an intermediate crystalline phase, MOF-14,<sup>10</sup> which starts to decompose at longer reaction times, and CAU-1,<sup>11</sup> which was shown quantitatively to form within a few minutes.<sup>12</sup>

Porphyrin-based linker molecules have been intensively investigated in the synthesis of MOFs since the resulting porphyrin-based MOFs are often redox active. They have been used in catalysis<sup>13-19 20,21</sup> and were also tested for the singlet oxygen production in biomedical and non-medical applications as well as cancer therapy.<sup>22-24</sup> MOFs containing tri- or tetravalent cations are known for their high stability,<sup>25</sup> and in combination with 4-tetracarboxyphenylporphyrine (H<sub>6</sub>TCPP), which is the most intensively investigated porphyrin-linker in MOF synthesis,<sup>26-28</sup> various compounds exhibiting permanent porosity have been reported. First pioneering work in the field of porphyrin-based MOFs incorporating the H<sub>6</sub>TCPP ligand were carried out by Suslick et al. and Goldberg et al. in 2000 and 2002.<sup>29,30</sup> More recent studies led to Zr-MOFs known as PCN-221 to -225,<sup>13,31,14,32</sup> MOF-545,<sup>33</sup> and MOF-525.<sup>33,34</sup> Some of these compounds have been tested in various catalytic reactions, such as the oxidation of cyclohexane,<sup>35</sup> the electrochemical reduction of CO<sub>2</sub>,<sup>16</sup> or the photooxidation of mustard gas.<sup>19</sup> A larger variety of porphyrin-based MOFs is known with trivalent ions. Thus three isorecticular MOFs with the group 13 metal ions aluminum, gallium and indium (Al-PMOF,<sup>36</sup> Ga-PMOF,<sup>37</sup> In-PMOF)<sup>37</sup> have been reported, and

the Al-PMOF was investigated in the photocatalytic methyl viologen assisted H<sub>2</sub>-generation on colloidal platinum.<sup>36</sup> In addition, porphyrin-based In-MOFs (MMPF-7,<sup>38</sup> MMPF-8<sup>38</sup> and UNLPF-10<sup>39,40</sup>), Fe-MOFs (MIL-141,<sup>41</sup> [Fe<sub>2</sub>(Fe-TCPP)(C<sub>4</sub>H<sub>4</sub>N<sub>2</sub>)(OH<sub>2</sub>)] (C<sub>4</sub>H<sub>4</sub>N<sub>2</sub> = pyrazine),<sup>42</sup> and PCN-600)<sup>43</sup> and MOFs containing lanthanide ions like Ce,<sup>44,45</sup> Nd,<sup>46</sup> Sm<sup>47</sup> and Dy<sup>46</sup> are also known. For the latter examples, only the crystal structures but no physisorption measurements were reported.

Herein we present the results of our systematic investigation on the synthesis of twelve trivalent Ce-MOFs using the porphyrin-based linker H<sub>6</sub>TCPP in the absence and presence of various benzoic acid derivatives (HBA-X, X = H, Cl, NH<sub>2</sub>, NO<sub>2</sub>, COOH) that can act as a co-ligand (Fig. 1), their structural transformation upon activation as well as the results of our *in situ* crystallization studies.

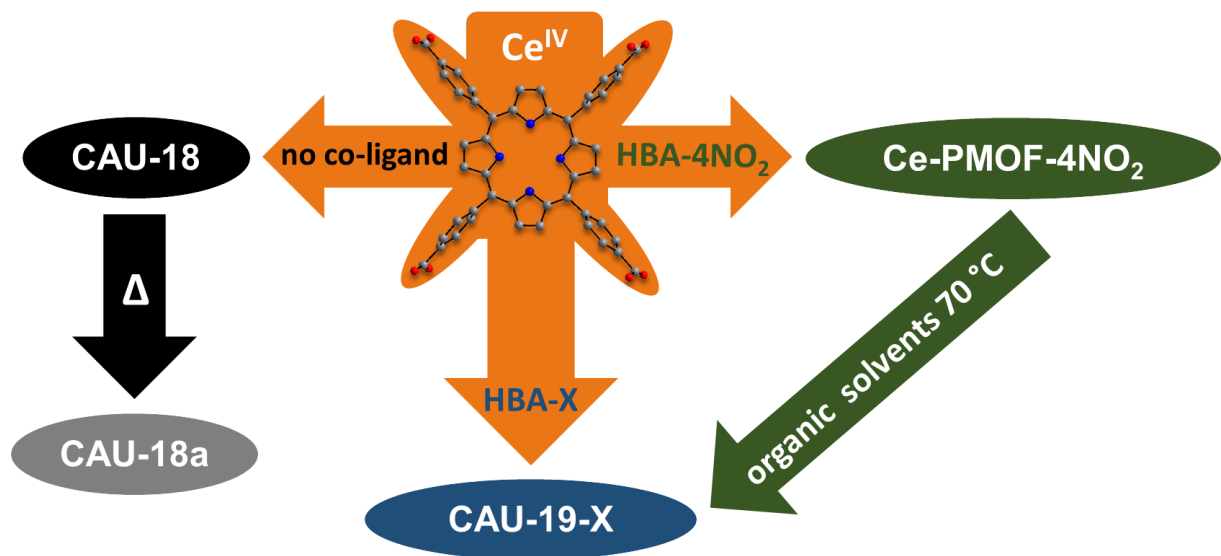


**Figure 1.** Graphical representation of the investigation of the system Ce<sup>4+</sup> / H<sub>6</sub>TCPP / DMF / H<sub>2</sub>O in the absence or presence of benzoic acid derivatives (HBA-X, X = H, Cl, NH<sub>2</sub>, NO<sub>2</sub>, COOH) as co-ligands. The study led to the new porphyrin-based Ce-MOFs CAU-18, CAU-18a, CAU-19-X (X= H, 2Cl, 3Cl, 4Cl, 4NH<sub>2</sub>, 4NO<sub>2</sub>, 3CO<sub>2</sub>H) and Ce-PMOF-4NO<sub>2</sub>.

## Experimental section

**Materials.** Cerium(IV) ammonium nitrate ( $(\text{NH}_4)_2[\text{Ce}(\text{NO}_3)_6]$ ) (98 %, ABCR), benzoic acid (99.5 %, ABCR), 2-chlorobenzoic acid (98 %, ABCR), 3-chlorobenzoic acid (99 %, Sigma Aldrich), 4-chlorobenzoic acid (99 %, Sigma Aldrich), 3-carboxybenzoic acid (trimellitic acid, 99 %, Sigma Aldrich), 4-aminobenzoic acid (99 %, Sigma Aldrich), 4-nitrobenzoic acid (99 %, ABCR),  $\text{ZnSO}_4 \cdot \text{H}_2\text{O}$  (97 %, Merck),  $\text{CoCl}_2 \cdot 6 \text{H}_2\text{O}$  (98 %, Fluka), dimethylformamide (DMF, 99 %, Grüssing), acetone (99 %, Walther), methanol (99 %, Walther), dichloromethane (DCM, 99 %, Walther) and ethanol (99 %, Walther) were used without further purification. The cerium(IV) ammonium nitrate was dissolved in distilled  $\text{H}_2\text{O}$  to achieve a 0.53 M solution. The linker 4,4',4'',4'''-(5,10,15,20-porphyrinetetrayl)tetrabenzoic acid (4-tetracarboxyphenylporphyrin,  $\text{H}_6\text{TCPP}$ ) was synthesized according to reported procedures<sup>48–50</sup> starting with 4-formylbenzoic acid (98 %, ABCR) and pyrrole (98 %, ABCR) in propionic acid (99 %, Grüssing). The metalated linker Co- $\text{H}_4\text{TCPP}$  was synthesized according to reported procedures. First Co- $\text{TCPP-Me}_4$ <sup>51</sup> was obtained by reaction of  $\text{H}_6\text{TCPP}$  with  $\text{CoCl}_2 \cdot 6 \text{H}_2\text{O}$  in MeOH which was subsequently hydrolysed.<sup>52</sup> Details are given in the Supporting Information.

## Characterization.

Single crystal X-ray diffraction data for CAU-18 and CAU-19-H were acquired at the beamline ID11 at ESRF (Grenoble, France). The reflections were indexed with the APEX3 suite, integrated with SAINT V9.32B,<sup>53</sup> solved with the program SHELXL,<sup>54</sup> and refined with the

program SHELXL using Olex2 as GUI.<sup>55</sup> A radiation energy of 40 keV was used, corresponding to a wavelength of  $\lambda=0.3112$  Å. The non-standard wavelength induced a checkcif warning due to mismatch of the determined and calculated absorption coefficient  $\mu$ . Only one full hemisphere ( $\phi$  scan) was collected for each sample, due to time constraints, resulting in non-complete data sets. Both crystals were very small and poorly diffracting, and in addition suffered from radiation damage during the measurements. Both structures contain stacked porphyrin rings, likely to cause stacking disorder in the crystals. This disorder is likely to have caused the poor precision on bond lengths and ADP values in the obtained crystal structures. Restraints forcing ADP tensor components to approximate to isotropic behavior (isor) and rigid body restraints (rigu) were used to prevent unphysical ADP values.

All Ce L<sub>3</sub>-edge XANES measurements, except for Ce(NO<sub>3</sub>)<sub>3</sub> · 6 H<sub>2</sub>O, were performed at the Southern Federal University (Rostov-on-Don, Russia) using a Rigaku R-XAS spectrometer. The water-cooled X-ray tube with a fixed W anode was operating at 12 kV and 80 mA. The incident beam was monochromatized using a Johansson-type Ge (220) crystal, ensuring an energy resolution of around 1 eV at 5730 eV. The measurements were conducted in transmission mode using an Ar-filled ionization chamber and a scintillation counter to monitor the intensity of incident ( $I_0$ ) and transmitted ( $I_1$ ) radiation respectively. A He-filled bag was placed between the X-ray tube, the monochromator and the  $I_0$  detector to reduce the X-rays absorption in air. The spectrum of Ce(NO<sub>3</sub>)<sub>3</sub> · 6 H<sub>2</sub>O was collected at the BM23 beamline of the European Synchrotron Radiation Facility (Grenoble, France) in transmission mode using a Si (111) crystal for monochromatization, Si mirrors for harmonics rejection and N<sub>2</sub>/He-filled ionization chambers for photon detection, yielding resolution comparable with the laboratory measurement. In all cases the samples were measured in the form of self-supporting pellets mixed with boron nitride

and pressed with a pressure below 400 kg/cm<sup>2</sup>. Mass of the samples was optimized by using the XAFSmass code<sup>56</sup> to obtain the best signal-to-noise ratio.

PXRD measurements were carried out with a STOE HT diffractometer equipped with a xy-stage and an IPDS (Cu K $\alpha_1$  radiation) or Mythen (Mo K $\alpha_1$  radiation) detector system. High resolution PXRD patterns were measured on a STOE Stadi-P combi powder diffractometer equipped with a Mythen detector (Cu K $\alpha_1$  radiation). The structure of Ce-PMOF-4NO<sub>2</sub> was refined from PXRD data using the Rietveld method. Only an approximated structure model was obtained due to broad reflections with a low signal to noise ratio and the presence of small amounts of CAU-19-4NO<sub>2</sub>. An appropriate structure model for CAU-18a could not be set up due to limited long range order in the sample. Nevertheless, the PXRD pattern of CAU-18a could be indexed using TOPAS academic V4.1<sup>57</sup> and a unit cell similar to CAU-18 was found and confirmed by a Pawley-fit (Table 2 and Figure S20). Pawley-fits (Fig. S22 – S29) were carried out for all other CAU-19-X and M-CAU-19-H (M= Zn, Co) derivatives to proof that they are isostructural to CAU-19-H. Pawley-fits of CAU-18 and CAU-19-H (Fig. S19 and S21) with the lattice parameters determined from the single crystal structure determination were carried out to proof the phase purity. Pawley-fits and Rietveld-refinements were performed with the program TOPAS academic V4.1.<sup>57</sup> The results of the refinement and crystallographic data of CAU-18, CAU-18a, CAU-19-H and Ce-PMOF-4NO<sub>2</sub> is shown in Table 2. The refined cell parameters and results of the Pawley-fits of the other CAU-19-X and M-CAU-19-H (M= Zn, Co) derivatives are shown in Table S2 and S3 and Figure S19 – S29. The diameters of all pores were determined using DIAMOND V.3<sup>58</sup> taking the van-der-Waals radii of the atoms into account. The VT-PXRD measurements were recorded on a STOE Stadi-P combi powder diffractometer (Cu K $\alpha_1$  radiation: CAU-18; Mo K $\alpha_1$  radiation: CAU-19-H) equipped with a capillary furnace. For the



measurements 0.5 mm quartz capillaries were used. The samples were heated up in steps of 5 K to 500 and 600 °C for CAU-18 and CAU-19-H, respectively, and measured for 10 minutes each.

The *in situ* PXRD measurements were carried out at beamline P09<sup>59</sup> ( $\lambda=0.53905$  Å) and P07B<sup>60</sup> ( $\lambda=0.14235$  Å) at PETRA III, DESY, Hamburg. The sample-to-detector distance was 606.074 mm and 2682.568 mm at P09 and P07B, respectively. In both cases a Perkin Elmer 1621 Flat Panel Detector (2048 x 2048 pixel; 200µm x 200µm pixel size) was used. At beamline P09<sup>59</sup> the experiments were executed with a beam size of 1 x 1 mm. At beamline P07B<sup>60</sup> the beamsizes were set to 0.5 x 0.5 mm. The reactions were carried out in a custom-built reactor that was developed at CAU Kiel in cooperation with the beamline staff of beamline P08, PETRA III, DESY.<sup>61</sup> The reactor was designed to enable the analysis of chemical reactions under solvothermal reaction conditions *via* synchrotron based techniques. The core of the reactor consists of an aluminum casing surrounded by copper-galvanized heating wires. Reaction vessels made from borosilicate glass ( $V_{\text{max}} = 5$  ml) can be inserted into the casing that is aligned in transmission geometry on the beamline. The temperature inside the reaction vessel was constantly monitored throughout the entire reaction by means of a PTFE-coated k-type thermocouple. Through a combination of resistive heating from the heating wires and direct cooling of the heating wires *via* compressed air the temperature inside the glass vessel was precisely controlled with a deviation of  $\pm 0.5$  °C. A stirring device under the base of the reactor allowed for homogenization of the sample during the reaction. The setup furthermore provides the option of adding solutions during the reaction by means of a remote-controlled syringe pump. The syringe pump system is connected to PTFE-tubes that are embedded in the custom-built screw caps. In this study the syringe pump was used to start the reactions remotely that lead to the formation of CAU-19-H. To ensure a constant reaction temperature the linker solution was

first heated to the target temperature followed by the injection of metal salt solution to start the reaction. A more detailed description of the experiment procedure is provided in the section discussing the *in situ* studies.

IR-spectra were recorded using a Bruker ALPHA-FT-IR A220/D-01 spectrometer equipped with an ATR-unit. UV/vis spectra were recorded at a Spectroquant Pharo 300 M. Prior to the measurements all samples were dissolved in 2M NaOH and measured at once.  $^1\text{H}$ -NMR spectroscopy was employed for the quantitative analysis of occluded guest molecules and co-ligands. The NMR spectra were recorded on a Bruker DRX 500 spectrometer. The samples were dissolved in a mixture of 10 % deuteriochloric acid (DCl) in  $\text{D}_2\text{O}$  and deuterated dimethyl sulphoxide ( $\text{d}_6$ -DMSO) (molar ratio=1:7). Sorption experiments were performed with a BEL Japan Inc. BELSORP-max. Before sorption measurements all samples were activated at 170 °C under reduced pressure ( $10^{-2}$  kPa) for 16 h. Thermogravimetric measurements were performed on a NETZSCH STA 409 CD analyzer under a flow of air ( $75 \text{ ml min}^{-1}$ ) with a heating rate of  $4 \text{ }^\circ\text{C min}^{-1}$  between 25 and 700 °C in  $\text{Al}_2\text{O}_3$ -crucibles. The data were corrected for buoyancy and current effects.

**Preparation.** The syntheses of CAU-18 and CAU-19-X (X=H, 2Cl, 3Cl, 4Cl, 3CO<sub>2</sub>H, 4NH<sub>2</sub>, 4NO<sub>2</sub>) were carried out in glass-vials ( $V_{\text{max}} = 7.0 \text{ mL}$ , Pyrex) using a solvent mixture (volume ratio H<sub>2</sub>O to DMF of 1 to 3). Ce-PMOF-4NO<sub>2</sub> was obtained in 30 mL autoclaves with Teflon inserts using DMF as solvent and 4-nitrobenzoic acid as co-ligand. For the synthesis optimization reactions were carried out between 80 and 140 °C, at reaction times between 1 and 48 h using different molar ratios of metal : linker : HBA-X between 1 : 1 : 0 and 5 : 1 : 300

(HBA-X = C<sub>7</sub>H<sub>4</sub>O<sub>2</sub>-X, X= X=H, 2Cl, 3Cl, 4Cl, 3CO<sub>2</sub>H, 4NH<sub>2</sub>, 4NO<sub>2</sub>). The formation of the metalated compounds M-CAU-19-H (M= Zn, Co) was investigated starting from the synthesis conditions of CAU-19-H. In case of Zn-CAU-19-H the addition of ZnSO<sub>4</sub> · H<sub>2</sub>O and a reaction time of 1 h resulted in the formation of Zn-CAU-19-H. Co-CAU-19-H was obtained by an increase of metal to linker ratio to 5:1 and a higher amount of DMF (2400 µL). Activation of the samples was carried out by thermal treatment or by a combination of solvent exchange at elevated temperatures followed by thermal treatment under reduced pressure.

The optimized synthesis parameters of all title compounds are summarized in Table 1 and the results of the elemental analyses are given in Table S1. The detailed synthesis procedures for CAU-18, CAU-18-HT, CAU-19-H, M-CAU-19-H (M=Zn, Co) and Ce-PMOF-4NO<sub>2</sub> are as follows:

**CAU-18:** H<sub>6</sub>TCPP (20 mg, 2.53 x 10<sup>-2</sup> mmol), DMF (1200 µL), H<sub>2</sub>O (300 µL) and 0.53 M aqueous (NH<sub>4</sub>)<sub>2</sub>[Ce(NO<sub>3</sub>)<sub>6</sub>] solution (94 µL, 5.06 x 10<sup>-2</sup> mmol) were added to a 7.0 mL glass vial. The glass vial was heated for 2 h at 100 °C. The resulting product was filtered off and washed two times each with DMF and acetone. A yield of 63 mg, (79 % based on H<sub>6</sub>TCPP) was obtained for CAU-18, [Ce<sub>4</sub>(H<sub>2</sub>TCPP)<sub>3</sub>(DMF)<sub>2</sub>(H<sub>2</sub>O)<sub>4</sub>].

**CAU-18a:** CAU-18 (500 mg, 0.16 mmol) was placed in a crucible and heated for 24 h at 250 °C. A yield of 470 mg, 100 % was obtained for CAU-18a, based on the composition [Ce<sub>4</sub>(H<sub>2</sub>TCPP)<sub>3</sub>] · 22 H<sub>2</sub>O deduced from elemental analysis and TG measurement.

**CAU-19-H:** H<sub>6</sub>TCPP (20 mg, 2.53 x 10<sup>-2</sup> mmol), benzoic acid (HBA-H) (570 mg, 4.67 mmol), DMF (1200 µL), H<sub>2</sub>O (300 µL) and 0.53 M aqueous (NH<sub>4</sub>)<sub>2</sub>[Ce(NO<sub>3</sub>)<sub>6</sub>] solution (94 µL, 5.06 x 10<sup>-2</sup> mmol) were added to a 7.0 mL glass vial. The glass vial was heated for 24 h at

120 °C. The resulting product was filtered off and washed two times each with DMF and acetone. A yield of 16 mg, 56 % (based on H<sub>6</sub>TCPP) was obtained for CAU-19-H, [Ce<sub>3</sub>(H<sub>2</sub>TCPP)<sub>2</sub>(BA-H)(HBA-H/H<sub>2</sub>O)<sub>2</sub>] · 2 (HBA-H) · 11 H<sub>2</sub>O.

**Zn-CAU-19-H:** H<sub>6</sub>TCPP (20 mg, 2.53 x 10<sup>-2</sup> mmol), ZnSO<sub>4</sub> (5 mg, 3.10 x 10<sup>-2</sup> mmol), benzoic acid (HBA-H) (570 mg, 4.67 mmol), DMF (1200 µL), H<sub>2</sub>O (300 µL) and 0.53 M aqueous (NH<sub>4</sub>)<sub>2</sub>[Ce(NO<sub>3</sub>)<sub>6</sub>] solution (94 µL, 5.06 x 10<sup>-2</sup> mmol) were added to a 7.0 mL glass vial. The glass vial was heated for 1 h at 120 °C under stirring. The resulting product was filtered off and washed two times each with DMF and acetone. A yield of 15 mg, 53 % (based on H<sub>6</sub>TCPP) was obtained for Zn-CAU-19-H, [Ce<sub>3</sub>(Zn-TCPP)<sub>2</sub>(BA-H)(HBA-H/H<sub>2</sub>O)<sub>2</sub>] · 2 (HBA-H) · 8 H<sub>2</sub>O.

**Co-CAU-19-H:** Co-H<sub>4</sub>TCPP (20 mg, 2.53 x 10<sup>-2</sup> mmol), benzoic acid (HBA-H) (570 mg, 4.67 mmol), DMF (2400 µL), H<sub>2</sub>O (350 µL) and 0.53 M aqueous (NH<sub>4</sub>)<sub>2</sub>[Ce(NO<sub>3</sub>)<sub>6</sub>] solution (94 µL, 12.65 x 10<sup>-2</sup> mmol) were added to a 7.0 mL glass vial. The glass vial was heated for 2 h at 120 °C under stirring. The resulting product was filtered off and washed two times each with DMF and acetone. A yield of 12 mg, 42 % (based on Co-H<sub>4</sub>TCPP) was obtained for Co-CAU-19-H, [Ce<sub>3</sub>(Co-TCPP)<sub>2</sub>(BA-H)(HBA-H/H<sub>2</sub>O)<sub>2</sub>] · 2 (HBA-H) · 11 H<sub>2</sub>O.

To prove that the porphyrin linker is still metalated after the MOF synthesis UV/vis spectra (Fig. S4) were measured. Prior to the measurements all samples were dissolved in 2M NaOH. The measurements reveal no significant loss of Co<sup>2+</sup> and Zn<sup>2+</sup> ions. The absorption maxima of the linker molecules incorporated in CAU-19-H, Zn-CAU-19-H and Co-CAU-19-H after dissolution in 2 M aqueous NaOH solution were observed at 414, 422 and 430 nm, respectively and correspond well to values reported in the literature (H<sub>6</sub>TCPP=413,<sup>18,62</sup> Zn-H<sub>4</sub>TCPP=424 nm,<sup>63</sup> Co-H<sub>4</sub>TCPP=430 nm<sup>18</sup>).

To remove the non-coordinating solvent and HBA-X molecules from the as-synthesized samples, the materials were treated under reflux with acetone (CAU-19-X, with X = H, 2Cl, 4Cl, 4NH<sub>2</sub>, and M-CAU-19-H (M=Zn, Co)) or DMF (CAU-19-3Cl and CAU-19-3CO<sub>2</sub>H). This procedure was repeated until no further decrease of the amount of HBA-X was observed in the <sup>1</sup>H-NMR spectra (Fig. S5-S12).

**Ce-PMOF-4NO<sub>2</sub>:** H<sub>6</sub>TCPP (180 mg, 22.77 x 10<sup>-2</sup> mmol), 4-nitrobenzoic acid (HBA-4NO<sub>2</sub>) (2000 mg, 12.05 mmol), DMF (9000 μL) and 0.53 M aqueous (NH<sub>4</sub>)<sub>2</sub>[Ce(NO<sub>3</sub>)<sub>6</sub>] solution (850 μL, 45.54 x 10<sup>-2</sup> mmol) were added to a 30 mL teflon vessel. The teflon vessel was placed in an autoclave and was heated for 48 h at 120 °C. The resulting product was filtered off and washed with 100 mL DMF. A yield of 139 mg, 44 % (based on H<sub>6</sub>TCPP) was obtained for Ce-PMOF-4NO<sub>2</sub>, [Ce<sub>2</sub>(H<sub>2</sub>TCPP)(BA-4NO<sub>2</sub>)<sub>2</sub>] · 2 DMF.

**CAU-19-4NO<sub>2</sub>:** Ce-PMOF-4NO<sub>2</sub> (500 mg, 0.36 mmol) and 30 mL acetone were placed in a 50 mL glass vessel with screw cap and heated in an oven for 72 h at 70 °C. A yield of 427 mg, 100 % was obtained for CAU-19-4NO<sub>2</sub> (yield calculated based on the linker molecule and corresponding to the formula [Ce<sub>3</sub>(H<sub>2</sub>TCPP)<sub>2</sub>(BA-NO<sub>2</sub>)(HBA-NO<sub>2</sub>/H<sub>2</sub>O)<sub>2</sub>] · 2 (HBA-NO<sub>2</sub>) · 6 H<sub>2</sub>O for CAU-19-4NO<sub>2</sub>).

**Table 1.** Summary and comparison of the synthesis parameters of CAU-18, CAU-19-X (X=H, 2Cl, 3Cl, 4Cl, 3CO<sub>2</sub>H, 4NH<sub>2</sub>) and Ce-PMOF-4NO<sub>2</sub>. All CAU-19-Cl derivatives were obtained using the same synthesis parameters. All syntheses were carried out in 7 mL glass vials except Ce-PMOF-4NO<sub>2</sub> which was synthesized in a 30 mL teflon reactor.

CAU	-18	-19-H	-19-Cl <sup>a</sup>	-19-4NH <sub>2</sub>	-19-3CO <sub>2</sub>	Ce-PMOF
<b>M : L : HBA-X<sup>b</sup></b>	1:2:0	1:2:180	1:2:150	1:2:200	1:2:140	9:18:450
<b>H<sub>2</sub>O : DMF<sup>c</sup></b>	1:3	1:3	1:3	1:3	1:3	2.8:30
<b>HBA-X [mg]</b>	-	570	600	700	600	2000
<b>T [°C]</b>	100	120	120	120	120	120
<b>t [h]</b>	2	24	2	24	24	48
<b>yield [%]</b>	79	56	51, 30, 72 <sup>a</sup>	75	37	44

<sup>a</sup> CAU-19-Cl indicates all CAU-19-Cl derivatives in following order 2Cl, 3Cl, 4Cl.

<sup>b</sup> molar ratio, the number 1 corresponds to  $2.53 \times 10^{-2}$  (20 mg) mmol

<sup>c</sup> volumetric ratio, the number 1 corresponds to 300  $\mu$ L H<sub>2</sub>O

## Results and Discussion

The systematic study employing the linker molecule 4-tetracarboxyphenylporphyrine ( $H_6TCPP$ ) as well as co-ligands ( $HBA-X$ , with  $X = H, 2Cl, 3Cl, 4Cl, 3CO_2H, 4NH_2, 4NO_2$ ) led to twelve new porphyrin-based Ce-MOFs. In contrast to previous studies in the group Goldberg, we used co-ligands in our syntheses which have a strong influence on the product formation.<sup>45</sup>

The synthesis of the porphyrin-based Ce-MOFs was investigated starting from the reaction procedures recently reported for the synthesis of Ce-UiO-66 and an In-MOF containing the  $H_2TCPP^{4-}$  ion.<sup>21,37</sup> The title compounds **CAU-18**,  $[Ce_4(H_2TCPP)_3(DMF)_2(H_2O)_4]$  and **CAU-19-X**,  $[Ce_3(H_2TCPP)_2(BA-X)(HBA-X/H_2O)_2] \cdot 2HBA \cdot 11H_2O$ , were obtained under very similar reaction conditions as described for the formation of Ce-UiO-66.<sup>21</sup> Thus  $(NH_4)_2[Ce(NO_3)_6]$  was used as the metal source, and the reaction was carried out using short reaction times ( $T_{max} = 2$  h), low reaction temperatures (100 -120 °) and a DMF/ $H_2O$  solvent mixture (3:1). Although the formation of a hexanuclear  $\{Ce_6O_8\}$  cluster and therefore the crystallization of compounds isostructural to the known porphyrin-based Zr-MOFs<sup>34</sup> was anticipated, this approach resulted in the formation of new Ce-MOFs with dimeric and trimeric IBUs that are connected by the  $H_2TCPP^{4-}$  ions to form three-dimensional framework structures. **CAU-18** is formed in the absence of a co-ligand, while **CAU-19-H** was obtained in the presence of benzoic acid (HBA). Subsequently, usage of different benzoic acid derivatives ( $HBA-X$ , with ( $X=H, 2Cl, 3Cl, 4Cl, 3CO_2H, 4NH_2$ )) resulted in the formation of a series of CAU-19 type compounds with the  $BA-X^-$  ions incorporated into the crystal structure. While the molar ratio  $Ce^{4+}$  to  $H_6TCPP$  has the most pronounced impact on the product formation, the amount of co-ligand varies slightly (Tab. 1). Unexpectedly, the use of 4-nitrobenzoic acid ( $HBA-NO_2$ ) as a co-ligand and the increase of the

DMF to H<sub>2</sub>O ratio from 3:1 to 9:1 results in the formation of the new Ce-MOF [Ce<sub>2</sub>(H<sub>2</sub>TCPP)(BA-4NO<sub>2</sub>)<sub>2</sub>] · 2DMF (**Ce-PMOF-4NO<sub>2</sub>**).

**Activation of the Ce-MOFs.** Thermal activation and variable-temperature PXRD measurements of the title compounds revealed several structural changes. Thus, the thermal treatment of **CAU-18** at 250 °C leads to a desolvated compound denoted **CAU-18a**. Activation of **Ce-PMOF-4NO<sub>2</sub>**, was carried out in a two-step process by treatment with an organic solvent at elevated temperatures, followed by thermal treatment under reduced pressure. The first step leads to the transformation of **Ce-PMOF-4NO<sub>2</sub>** into **CAU-19-4NO<sub>2</sub>** within 72 h at 70 °C. It is noteworthy that we have only been able to obtain **CAU-19-4NO<sub>2</sub>** by this treatment.

**Crystal Structure.** The title compounds CAU-18 and CAU-19-H were obtained as single crystals (Fig. S13, and S14), while all other MOFs were only synthesized as microcrystalline powders. Hence the structure of CAU-18 and CAU-19-H were determined from single crystal X-ray diffraction data, while the one of Ce-PMOF-4NO<sub>2</sub> was refined from PXRD data (Fig. 5, Tab. 2). In addition Pawley fits were carried out to determine the lattice parameters and to confirm phase purity of all title compounds (Fig. S19-S29, Tab. S2-S3).

**CAU-18** is isostructural to [Sm<sub>4</sub>(H<sub>2</sub>TCPP)<sub>3</sub>(DMF)<sub>2</sub>(H<sub>2</sub>O)<sub>4</sub>].<sup>47</sup> The IBU consists of edge-sharing CeO<sub>7</sub> and CeO<sub>9</sub> polyhedra, in a monocapped trigonal prismatic and a distorted tricapped trigonal prismatic coordination environment (Fig. 2). Each CeO<sub>7</sub> polyhedron contains one DMF molecule and each CeO<sub>9</sub> polyhedron two water molecules, the other oxygen atoms stem from carboxylate groups. The dimers are bridged to tetramers by carboxylate groups (Fig. 2) and further interconnection by H<sub>2</sub>TCPP<sup>4-</sup> ions leads to a three dimensional framework with very small pores of 2.4 x 5.0 Å which are too small to accommodate guest molecules (Fig. 2).



Adjacent tetramers approach each other along [101] to a distance of 3.13(3) Å, which hints at the presence of a weak H-bond interaction between a coordinated water molecule and an oxygen atom of a carboxylate group (Fig. S15). The coordination modes of the carboxylate groups in CAU-18 are shown in Fig. S16 using the Harris-notation.<sup>64</sup> The Harris-notation has the format [A,XY], the value A is the number of metal ions coordinated by the carboxylate group and X, Y is the number of bonds every oxygen shares with a metal ion.<sup>64</sup> In the structure of CAU-18 the coordination modes [2,21], [2,11], [1,11], [1,10] are observed.

The bond lengths found in CAU-18 are in good agreement with the literature values. For the Ce-O bonds values between 2.296(10) (CN: 7) and 2.841(7) Å (CN: 9) were found which are in good agreement with the literature value of 2.386(8) (CN:7) and 2.797(7) Å (CN:9).<sup>45,65</sup> The C=C double bond length varies between 1.319(14) (arom. phenyl) and 1.481(11) Å (arom. pyrrole) and the N=C double bond length between 1.323(12) and 1.349(10) Å which are also in good agreement with the literature values of 1.303(9) to 1.508(6) Å and 1.358(6) to 1.383(6) Å, respectively.<sup>33,45</sup>

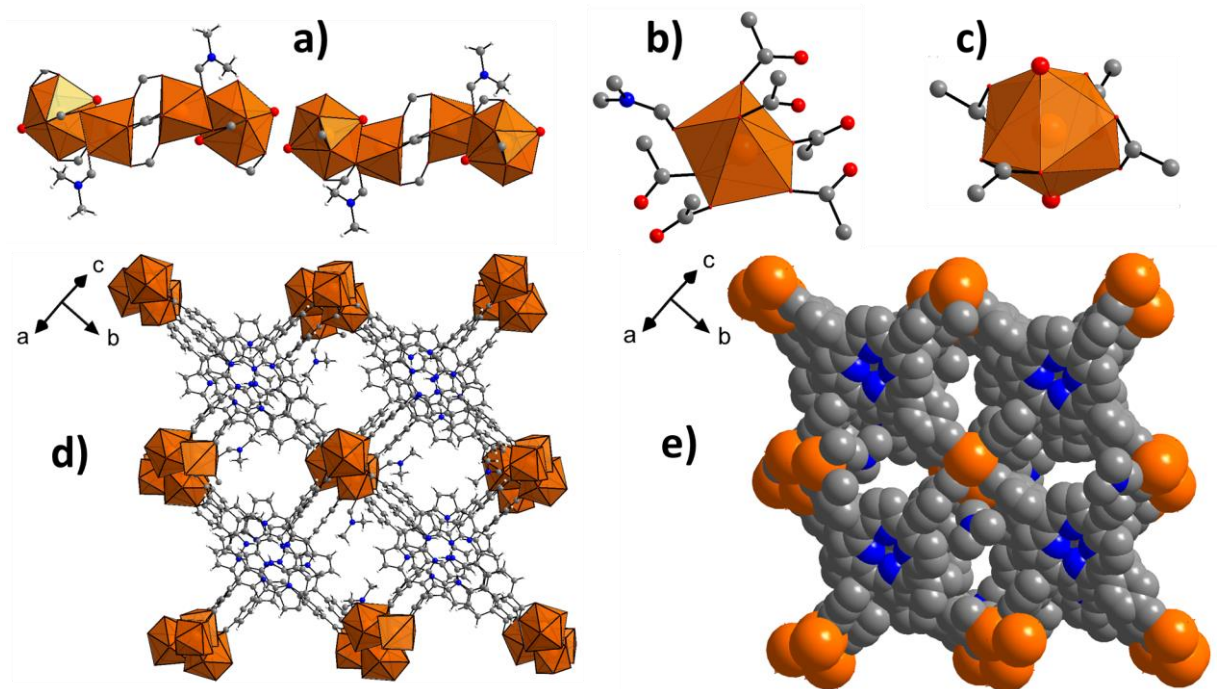


**Figure 2.** Structure of CAU-18. a) IBUs composed of edge-sharing  $\text{CeO}_7$  and  $\text{CeO}_9$  polyhedra with bridging  $-\text{COO}^-$  groups and coordinated DMF and water molecules, b)  $\text{CeO}_7$  polyhedron and coordination environment, c)  $\text{CeO}_9$  polyhedron and coordination environment, d) view of the framework structure e) space filling model of CAU-18. Carbon atoms are shown in grey, oxygen atoms in red, nitrogen atoms in blue and cerium atoms/ $\text{CeO}$  polyhedra in orange.

**CAU-19**,  $[\text{Ce}_3(\text{H}_2\text{TCPP})_2(\text{BA-X})(\text{HBA-X}/\text{H}_2\text{O})]$ , can be synthesized with different benzoic acid derivatives ( $\text{HBA-X}$ ,  $\text{X} = \text{H}, 2\text{Cl}, 3\text{Cl}, 4\text{Cl}, 4\text{NH}_2, 3\text{CO}_2\text{H}$ ) which are part of the structure (Fig. 3). The IBU contains trimers which are formed by edge-sharing of two  $\text{CeO}_8$  and one  $\text{CeO}_{12}$  polyhedra, in a distorted square antiprismatic and a distorted icosahedral coordination environment.

The co-ligands are incorporated as the benzoic acid derivative ([1,10] mode) as well as the anion ([1,11] mode)(Figure 3 b) and c)). The trimeric IBUs are connected to chains along [100] by  $\text{H}_2\text{TCPP}^{4-}$  ions (Fig. 3) which also connect the chains to a three-dimensional framework structure with linear oval channels along [100]. These pores have diameters of  $3.4 \times 8.8 \text{ \AA}$  and are accessible to guest molecules (Fig. 3). In the as synthesized compounds the pores are occupied by HBA-X molecules, which are, based on the single crystal X-ray diffraction data, located in two positions with an occupancy of 0.5 each (Fig. S17a, omitted for clarity in Fig. 3e). The non-coordinating HBA-X molecules can be removed by solvent extraction followed by thermal activation. The coordination mode of the carboxylate groups of CAU-19-H are shown in Fig. S17.<sup>64</sup>

The bond lengths found in CAU-19-H are in good agreement with the literature values. For Ce-O bonds, values between  $2.374(8)$  and  $2.730(6) \text{ \AA}$  were found, which are in good agreement with the literature values of  $2.413(4)$  to  $2.618(4) \text{ \AA}$  (CN: 8)<sup>45</sup> and  $2.364(5)$  to  $2.765(2) \text{ \AA}$  (CN: 12).<sup>45,65</sup> The C=C double bond length varies between  $1.327(13) \text{ \AA}$  (arom. phenyl) and  $1.512(11) \text{ \AA}$  (arom. pyrrole) and the N=C double bond length between  $1.348(11) \text{ \AA}$  and  $1.379(10) \text{ \AA}$  which are also in good agreement with the literature values of  $1.303(9) \text{ \AA}$  to  $1.508(6) \text{ \AA}$  and  $1.358(6) \text{ \AA}$  to  $1.383(6) \text{ \AA}$ , respectively.<sup>33,45</sup>

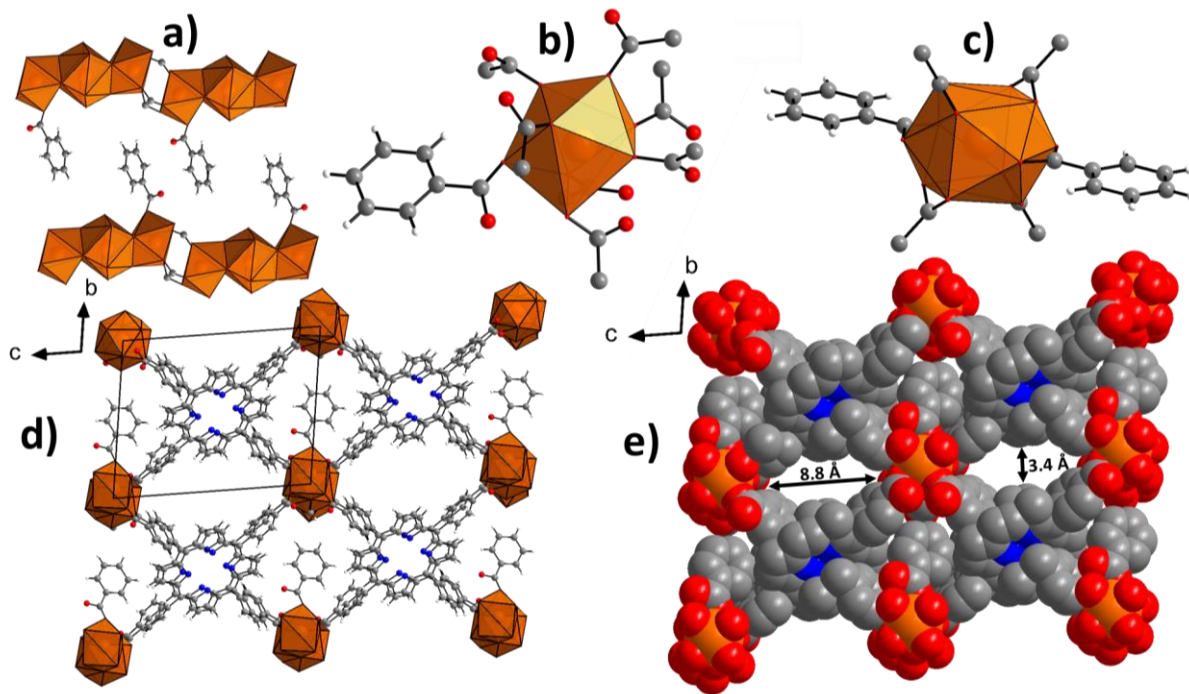


**Figure 3.** a) IBU of CAU-19-H along [010], b)  $\text{CeO}_8$  polyhedron and coordination environment, c)  $\text{CeO}_{12}$  polyhedron and coordination environment, d) view along pores [100] with unit cell edges and e) space filling model along [100] of CAU-19-H with pore diameters of 3.4/ 8.8 Å. Carbon atoms are shown in grey, oxygen atoms in red, nitrogen atoms in blue and cerium atoms /  $\text{CeO}$  polyhedra in orange.

Only one other porphyrine-based Ce-MOF of composition  $[\text{Ce}_3(\text{H}_2\text{TCPP})_2(\text{HCOO})(\text{H}_2\text{O})_3]$  has been previously reported in the literature.<sup>45</sup> Its structure resembles some similarities to the one observed for CAU-19, but formate instead of benzoate ions are coordinated to the IBUs. In addition  $\text{CeO}_{10}$  instead of  $\text{CeO}_{12}$  polyhedra are incorporated in the trimeric IBUs which are interconnected by the linker molecules to form a framework similar to CAU-19.<sup>45</sup>

The structure of **Ce-PMOF-4NO<sub>2</sub>**,  $[\text{Ce}_2(\text{H}_2\text{TCPP})(\text{BA-4NO}_2)_2] \cdot 2\text{DMF}$ , consists of chains of trans corner-sharing  $\text{CeO}_6$  polyhedra. The metal ions are bridged by the  $\mu$ -oxygen atom of the carboxylate group of 4-nitrobenzoic acid (Fig. 4). All other coordinating oxygen atoms stem

from the carboxylate groups of the  $\text{H}_2\text{TCPP}^{4-}$  ions. The chains are connected by  $\text{H}_2\text{TCPP}^{4-}$  molecules to form a three-dimensional framework. Two types of pores are formed along  $[010]$ , with pore diameters of  $5.0 \times 11.8 \text{ \AA}$  and  $2.0 \times 11.8 \text{ \AA}$ , respectively (Fig. 4). This structure is similar to the ones of  $[\text{M}_2(\mu\text{-OH})_2(\text{H}_2\text{TCPP})]$ ,  $\text{M} = \text{Al}, \text{Ga}$  and  $\text{In}$ <sup>36,37</sup> where the bridging of the  $\text{M}^{3+}$  ions is accomplished through  $\mu\text{-OH}$  groups. Since the  $\text{BA-NO}_2^-$  ion is not located on a special position, the occupancy of the co-ligand was constrained to 0.25.

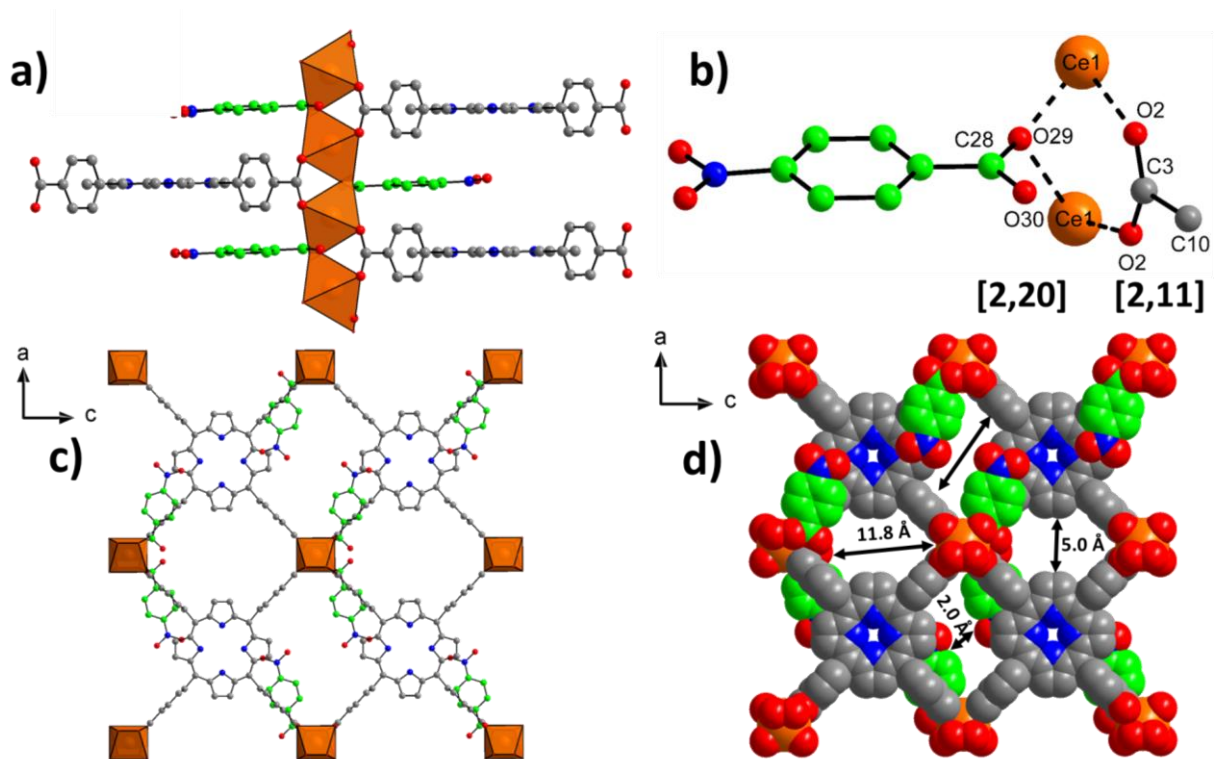


**Figure 4.** Structure of Ce-PMOF-4NO<sub>2</sub>. a) IBU along  $[100]$  with  $\text{BA-NO}_2^-$  ions as bridging groups between trans corner-sharing  $\text{CeO}_6$  polyhedra b) Harris notation in brackets for the carboxylate group of the co-ligand and the linker, c) view along pores  $[010]$  and d) space filling model along  $[010]$  with pore diameters of  $5.0 \times 11.8 \text{ \AA}$  and  $2.0 \times 11.8 \text{ \AA}$ , respectively. Carbon atoms are shown in grey, oxygen atoms in red, nitrogen atoms in blue and cerium atoms /  $\text{CeO}$  polyhedra in orange, for clarity the carbon atoms of the  $\text{BA-NO}_2^-$  ion are marked in green.

Thermal treatment of CAU-18 between 250 and 300 °C leads to a microcrystalline product, of composition  $[\text{Ce}_4(\text{H}_2\text{TCPP})_3]$ , denoted CAU-18a, with low long range order. At the activation temperature removal of coordinating  $\text{H}_2\text{O}$  and DMF molecules takes place and a permanently porous compound is formed which adsorbs 22  $\text{H}_2\text{O}$  molecules per formula unit. We anticipate condensation of the tetrameric units and formation of an open framework accessible for guest molecules. Thermogravimetric measurements confirm this hypothesis regarding the loss for DMF and  $\text{H}_2\text{O}$  molecules at 250 °C (Fig.8). IR spectroscopy confirms the absence of DMF molecules in CAU-18a (Fig. 11).

Since Ce(III) and Ce(IV) compounds exhibit very distinct Ce  $\text{L}_3$ -edge XANES features, the corresponding measurements were performed for all title compounds to probe the oxidation state of Ce ions, similarly to our previous Ce MOFs studies.<sup>21</sup> As demonstrated by comparison with the spectra of  $\text{CeO}_2$  and  $\text{Ce}(\text{NO}_3)_3 \cdot 6\text{H}_2\text{O}$  reference compounds presented in the Figure S18, all title compounds contain exclusively  $\text{Ce}^{3+}$  ions which were formed during the synthesis from the Ce(IV) precursor  $(\text{NH}_4)_2[\text{Ce}(\text{NO}_3)_6]$ . It is worth to note, that in the synthesis of Ce-UiO-66<sup>21</sup> the same reaction conditions were employed, but the tetravalent oxidation state was preserved during the reaction. Hence redox-active linker molecules such as  $\text{H}_6\text{TCPP}$  lead to the reduction of the  $\text{Ce}^{4+}$  ions during the reaction.

**Table 2.** Crystallographic data of CAU-18, CAU-18a, CAU-19-H and Ce-PMOF-4NO<sub>2</sub>.

	<b>CAU-18</b>	<b>CAU-18a</b>	<b>CAU-19 -H</b>	<b>Ce-PMOF -4NO<sub>2</sub></b>
<b>Formula</b>	[Ce <sub>4</sub> (H <sub>2</sub> TCPP) <sub>3</sub> (DMF) <sub>2</sub> (H <sub>2</sub> O) <sub>4</sub> ]	[Ce <sub>4</sub> (H <sub>2</sub> TCPP) <sub>3</sub> ]	[Ce <sub>3</sub> (H <sub>2</sub> TCPP) <sub>2</sub> (C <sub>7</sub> H <sub>4</sub> O <sub>2</sub> H) <sub>2</sub> (H <sub>2</sub> O) <sub>2</sub> ]	[Ce <sub>2</sub> (H <sub>2</sub> TCPP) (C <sub>7</sub> H <sub>4</sub> O <sub>2</sub> NO <sub>2</sub> ) <sub>2</sub> ]
<b>Data determined by</b>	single crystal	Pawley fit	single crystal	Rietveld refinement
<b>Crystal system</b>	monoclinic	monoclinic	triclinic	orthorhombic
<b><i>a</i> [Å]</b>	20.755(5),	22.420(3)	11.665(7)	33.077(3)
<b><i>b</i> [Å]</b>	23.572(6),	23.248(3)	13.915(8)	7.309(2)
<b><i>c</i> [Å]</b>	30.642(8)	34.419(5)	17.343(10)	16.539(2)
<b><i>α</i> [°]</b>	90	90	95.514(4)	90
<b><i>β</i> [°]</b>	104.573 (2)	106.375(5)	99.792(4)	90
<b><i>γ</i> [°]</b>	90	90	101.313(5)	90
<b><i>V</i> [Å<sup>3</sup>]</b>	14509(7)	17212(4)	2696(3)	3998(1)
<b>Space group</b>	<i>C2/c</i>	<i>P2/c</i>	<i>P</i> $\bar{1}$	<i>Cmmm</i>
<b>Tot., uniq. data, <i>R</i><sub>int</sub></b>	21207, 12183, 0.073		10313, 9008 0.038	
<b>Observed data [<i>I</i> &gt; 2σ(<i>I</i>)]</b>	6622		6710	
<b><i>R</i><sub>1</sub>, w<i>R</i><sub>2</sub> (gt) [%]</b>	7.5, 18.0		7.8, 20.6	
<b>GOF</b>	0.97	1.19	1.04	1.24
<b><i>R</i><sub>wp</sub></b>		2.03		4.46

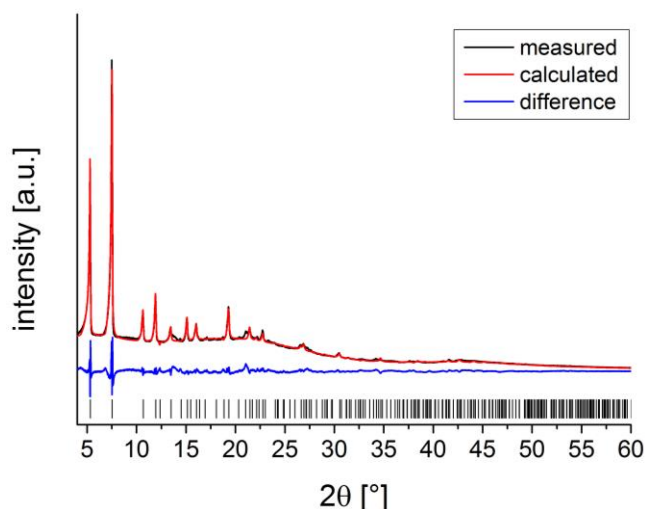


**Figure 5.** Result of the Rietveld-refinement of Ce-PMOF-4NO<sub>2</sub>. Measured data are shown as a black line, calculated data as a red line and the blue line gives the difference plot. Predicted peak positions are marked as vertical bars.

**Sorption Properties.** Sorption experiments were only carried out for CAU-18a, CAU-19-X and M-CAU-19-H (M=Zn, Co) since CAU-18 and Ce-PMOF-4NO<sub>2</sub> transform to CAU-18a and CAU-19-4NO<sub>2</sub> during the activation procedure. Prior to the sorption experiments all samples were activated at 170 °C under vacuum (10<sup>-2</sup> kPa) for 16 h. Subsequently sorption experiments using N<sub>2</sub> at 77 K (Fig. 6, S30 and S31) and H<sub>2</sub>O at 298 K (Fig. 7) as adsorptive were performed. The specific surface areas were determined using the BET method and applying the method of Roquerol.<sup>66,67</sup> Micropore volumes  $V_m$  were determined by using the amount of adsorbed N<sub>2</sub> at the relative pressure  $p/p_0 = 0.5$  (Table 3). All compounds are stable towards activation and sorption measurements as proven by PXRD measurements (Fig. S32). All N<sub>2</sub> measurements lead to a type-1a isotherm as expected for microporous materials with pore diameters  $\leq 1$  nm.<sup>67</sup> CAU-18a has a specific surface area of  $a_{BET} = 550 \text{ m}^2 \text{ g}^{-1}$  and the CAU-19-X derivatives have  $a_{BET}$  values between 330 and 600  $\text{m}^2 \text{ g}^{-1}$  depending on the incorporated co-ligand. The metalated forms of



CAU-19-H exhibit a specific surface area of 570 and 430 m<sup>2</sup> g<sup>-1</sup> for Zn-CAU-19-H and Co-CAU-19-H, respectively. If the specific surface areas per mmol are taken into account, the value of Zn-CAU-19-H is identical with the one of the non-metalated form, while for Co-CAU-19-H a slightly lower value is observed (Tab. 3).

A direct correlation of the steric demand of the different functional groups in CAU-19-X on the  $a_{BET}$  values is not observed. A co-ligand with a functional group in 2-position seems to lead to higher specific surface areas than ligands with groups in 3-, or 4-position (Tab. 3). CAU-19-4NH<sub>2</sub> has the smallest specific surface area of  $a_{BET}$  = 330 m<sup>2</sup> g<sup>-1</sup> which is due to the fact that not all HBA-NH<sub>2</sub> molecules could be removed from the pores during activation, as proven by NMR spectroscopy (Fig. S10, one HBA-NH<sub>2</sub> molecule per formula unit remains in the pores). The rather low specific surface area of CAU-19-4NO<sub>2</sub> of 400 m<sup>2</sup> g<sup>-1</sup> is due to the low long range order of the samples after the phase transformation.

The H<sub>2</sub>O sorption measurements at 298 K of all samples show an uptake between 10.7 and 21.3 wt% and CAU-18a exhibits the highest uptake of 21.3 wt%, followed by CAU-19-4NH<sub>2</sub> and CAU-19-3CO<sub>2</sub>H with values of 16.6 and 16.0 wt%. This result is remarkable since in the N<sub>2</sub> sorption experiments these latter MOFs showed the lowest N<sub>2</sub> uptake, but it is probably due to strong H-bond interactions between the amino- and the carboxy-group of the incorporated benzoic acid derivatives in the pores with the adsorptive water.

**Table 3.** Results of the sorption experiments ( $N_2$  at 77 K and  $H_2O$  at 298.15 K) of CAU-18a, CAU-19-X (X = H, 2Cl, 3Cl, 4Cl, 3CO<sub>2</sub>H, 4NH<sub>2</sub>, 4NO<sub>2</sub>) and M-CAU-19-H (M = Zn, Co). The micropore volume was calculated at  $p/p_0 = 0.5$ .

	CAU-18a	H	Zn H	Co H	2Cl	3Cl	4Cl	3CO <sub>2</sub> H	4NH <sub>2</sub>	4NO <sub>2</sub>
$N_2$ ( $a_{BET}$ ) [m <sup>2</sup> g <sup>-1</sup> ] [m <sup>2</sup> mmol <sup>-1</sup> ]	550 1620	600 1370	570 1374	430 1031	590 1390	580 1360	480 1130	490 1160	330 760	400 950
$N_2$ ( $V_m$ ) [cm <sup>3</sup> g <sup>-1</sup> ]	0.24	0.26	0.24	0.19	0.25	0.23	0.21	0.21	0.15	0.17
$H_2O$ (upt.) [mol mol <sup>-1</sup> ] [wt %]	34.8 21.3	25.7 14.1			19.8 10.7	26.8 14.4	26.4 14.2	30.0 16.0	30.4 16.6	23.0 12.3

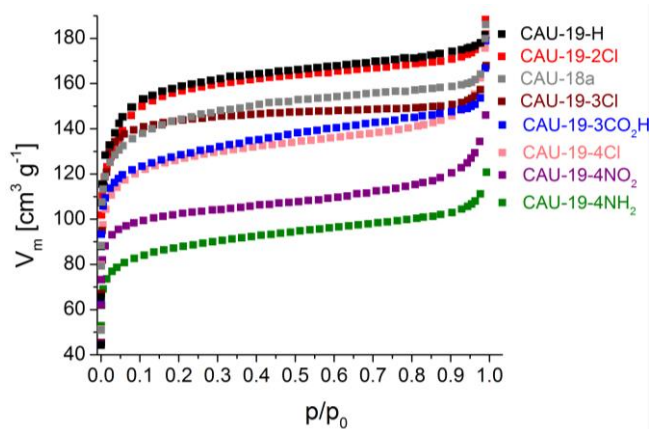


**Figure 6.**  $N_2$ -sorption isotherms of CAU-18a and CAU-19-X (X = H, 2Cl, 3Cl, 4Cl, 3CO<sub>2</sub>H, 4NH<sub>2</sub>, 4NO<sub>2</sub>) measured at 77 K. Only the adsorption branch is shown, desorption is omitted for clarity. All  $N_2$ -sorption isotherms including ad- and desorption are shown in the supporting information in Figure S30.

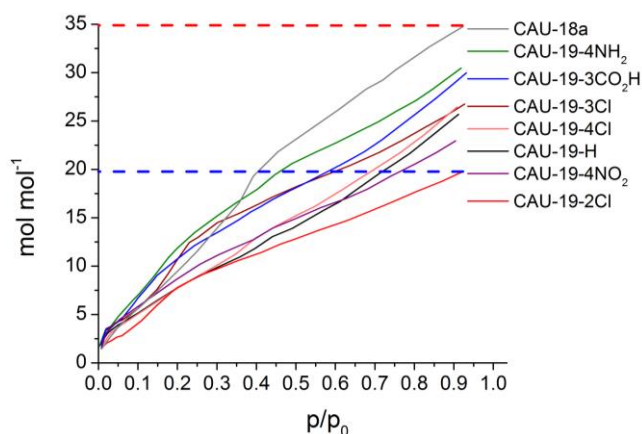


**Figure 7.** H<sub>2</sub>O sorption isotherms of CAU-18a and CAU-19-X (X = H, 2Cl, 3Cl, 4Cl, 3CO<sub>2</sub>H, 4NH<sub>2</sub>, 4NO<sub>2</sub>) measured at 298 K (mol mol<sup>-1</sup>). The red dashed line represents the sample with the highest uptake and the blue dashed line the sample with the lowest uptake, respectively.

**Thermal and Chemical Stability.** To investigate the thermal stability thermogravimetric (TG) measurements of all samples and variable temperature PXRD studies (VT-PXRD) for CAU-18 and CAU-19-H were carried out.

The results of the TG measurements (Table S4, Fig. 8 and 9 as well as Fig. S33 – S41) show two or three characteristic steps of weight loss, respectively. The loss up to 100 °C is assigned to the evaporation of physisorbed water molecules. In case of CAU-18 the removal of the coordinated DMF and water molecules occurs between 100 and 250 °C. The weight loss between 100 and 250 °C for CAU-19-3CO<sub>2</sub>H is due to the evaporation of physisorbed DMF as confirmed by <sup>1</sup>H-NMR spectroscopy (Fig. S9). Above 330 °C the decomposition of the compounds take place and CeO<sub>2</sub> is formed as the final product, as confirmed by PXRD measurements (Fig. S42). In the TG curve of CAU-18a three steps of weight loss are observed. The first two steps up to 150 °C can be assigned to the loss of water molecules. No further weight loss up to 330 °C is observed, when the framework starts to decompose. These results

demonstrate that the DMF molecules have been quantitatively removed during the transformation of CAU-18 to CAU-18a, which was also confirmed by elemental analysis. In general, the results of the TG analysis fit well with the ones of the elemental analyses. Slight differences in the amounts of occluded solvent molecules are due to the storage of the samples prior to the measurements where guest molecules can be exchanged by atmospheric water molecules.

The results of the VT-PXRD studies of CAU-18 and CAU-19-H are shown in Figure 10. These measurements show for CAU-18 two phase transformations one at 220 °C into an unknown intermediate and one at 300 °C into CAU-18a. Compared to the direct synthesis of CAU-18a (thermal treatment at 250 °C in air for 24 h) the phase transformation is delayed, probably due to the fact that the VT-PXRD measurements are performed in the confinement of the quartz capillaries within 4 h instead of an open crucible within 24 h. The unknown intermediate was also sometimes observed in the direct synthesis at 250 °C but after shorter reaction times of 2 h. A first decrease of crystallinity is observed up to 380 °C and the complete loss of crystallinity takes place at 490 °C. CAU-19-H shows a very similar behavior. Up to 380 °C no remarkable loss of crystallinity is observable but a few reflections are shifted during the measurement. A decrease of crystallinity is observable at 385 °C and the decomposition of the sample takes place at 480 °C. In comparison to the results of the TG the measurements show higher decomposition temperatures (CAU-18: 450-500 / 330 °C, CAU-19-H: 450-550 / 330 °C) which is due to the confinement of the sample in a capillary during the VT-PXRD measurements.

To investigate the chemical stability, CAU-18a and CAU-19-H were exemplarily treated in different solvents (2M HCl, 2M NaOH, 100 % acetic acid, H<sub>2</sub>O, MeOH, EtOH, acetone,

dichloromethane) at RT for 24 h under stirring. After the treatment the samples were isolated by filtration and measured by PXRD. The results of the chemical stability tests (Fig. S43) reveal that both MOFs are stable in all tested organic solvents and water, but show a complete decomposition in 2M HCl and 2M NaOH and decrease of crystallinity in 100 % acetic acid.

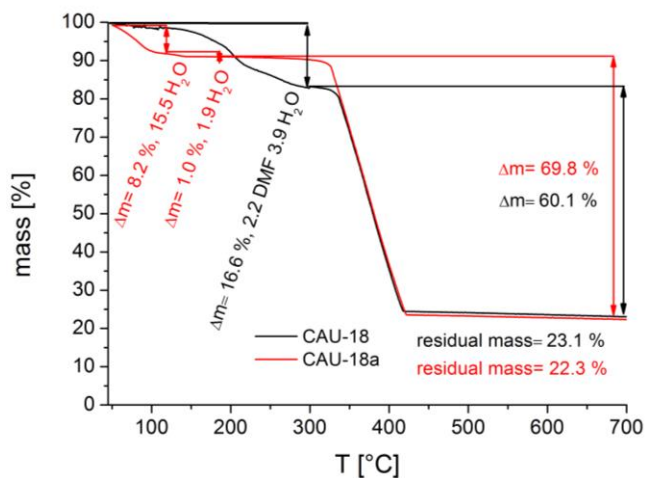


**Figure 8.** Thermogravimetric curve of CAU-18 ( $[\text{Ce}_4(\text{H}_2\text{TCCP})_3(\text{H}_2\text{O})_4(\text{DMF})_2]$ ) and CAU-18a ( $[\text{Ce}_4(\text{H}_2\text{TCCP})_3] \cdot 17.4\text{H}_2\text{O}$  (Table S4)).

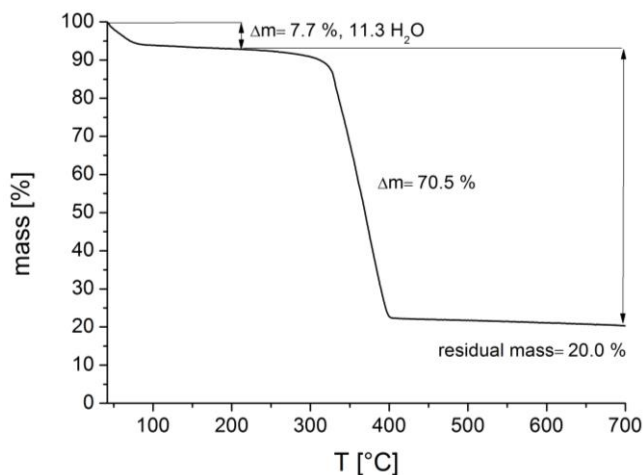


**Figure 9.** Thermogravimetric curve of CAU-19-H. Evaluation of the data reveals a molar ratio of metal : linker : benzoic acid : H<sub>2</sub>O of 3.1 : 2 : 4 : 11.3 (Table S4).

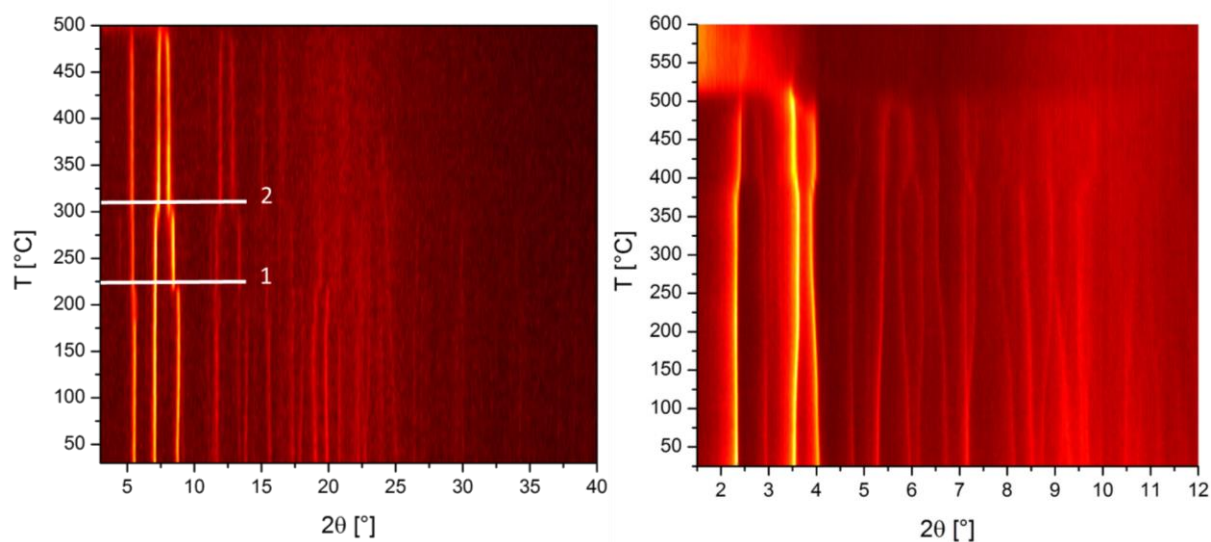


**Figure 10.** Results of the VT-PXRD studies of CAU-18 (left, Cu-K $\alpha_1$  radiation) and CAU-19-H (right, Mo-K $\alpha_1$  radiation) measured in open quartz capillaries (0.5 mm) under atmospheric conditions. The label 1 indicates the phase transformation into an unknown intermediate and the label 2 the phase transformation into CAU-18a.

### ***In situ* X-ray diffraction**

To learn more about the formation of CAU-18 and CAU-19-H *in situ* crystallization studies were carried out employing synchrotron radiation.<sup>68</sup> These MOFs are ideal candidates for such studies since they are formed within short reaction times of 1-2 h. In addition to the detection of possible crystalline intermediates X-ray diffraction (XRD) crystallization studies are a suitable method to determine kinetic parameters such as rate constants for nucleation ( $k_n$ ) and crystal growth ( $k_g$ ) as well as the respective Arrhenius activation energies ( $E_A$ ) and the probability of nucleation ( $P_n$ ) and have been reported for several MOFs like MIL-53,<sup>8</sup> MOF-14,<sup>10</sup> MIL-100<sup>9</sup> and CAU-13<sup>69</sup>. Crystallization studies have also been reported for other compounds which are obtained under solvothermal reaction conditions like zeolites,<sup>12</sup> polyoxovanadates<sup>70</sup> and thioantimonates.<sup>71</sup>

The crystallization of CAU-18 was carried out at three different reaction temperatures (110, 120 and 130 °C). The linker ( $H_6$ TCPP, 20 mg,  $2.53 \cdot 10^{-2}$  mmol), 2400  $\mu$ l N,N-dimethylformamid (DMF), 350  $\mu$ l dest.  $H_2O$  and 94.5  $\mu$ l of a 0.53 mol/L solution of  $(NH_4)_2[Ce(NO_3)_6]$  in dest.  $H_2O$  were placed in a borosilicate glass vessel ( $V_{max} = 5$  ml). After homogenization by shaking, the glass vessel was immediately placed into the reactor. The reaction mixture was heated to the target temperature within 3 min and stirred during the reaction while collecting powder diffraction data.

The *ex situ* crystallization study of CAU-19-H indicated a very fast formation. Hence the reactor was modified to include a syringe pump system which was employed to start the reaction remotely from the control hutch. The synthesis was carried out at three different reaction temperatures (120, 130 and 140 °C). A solution of  $H_6$ TCPP (20 mg,  $2.53 \cdot 10^{-2}$  mmol) and benzoic acid (550 mg, 4.5 mmol) in 2400  $\mu$ l DMF and 200  $\mu$ l  $H_2O$  was placed in a borosilicate glass

vessel ( $V_{\max} = 5$  ml) and heated to the target temperature (ca. 3 min) under stirring while continuously measuring XRD data. Subsequently 226  $\mu$ l of a 0.5333 mol/L solution of  $(\text{NH}_4)_2[\text{Ce}(\text{NO}_3)_6]$  in dest.  $\text{H}_2\text{O}$  was added *via* injection to initiate the reaction.

The results of the *in situ* crystallization of CAU-18 and CAU-19-H are shown for the reactions at 120 °C in Figure 11, further *in situ* crystallization plots are shown in Figures S44- S48. In order to investigate the kinetics of crystallization the normalized peak areas at the different reaction times, which correspond to the reaction progress  $\alpha$ , were determined. For CAU-18 the [020] and for CAU-19-H the [100] reflections were used, which are the ones with the highest intensity. The reaction progress  $\alpha$  at different reaction temperatures is shown in Figure 12. As expected, the induction time ( $t_{\text{ind}}$ ), in which no crystalline products are observed, and the total reaction time to achieve full conversion ( $t_{\text{com}}$ ) are shorter at higher temperatures (Fig. 12 and Tab. 4).

The method of Gualtieri was employed to determine the kinetic constants of the crystallization process of CAU-18 and CAU-19-H.<sup>12</sup> In this model the nucleation and the crystal growth are taken into account and are considered as separate processes (eqn. (1))

$$\alpha = \frac{1}{1 + \exp\left[-\left(\frac{t-a}{b}\right)^n\right]} \{1 - \exp(k_g t)^n\} \quad (1)$$

The reaction progress  $\alpha$  is a non-linear function depending on the reaction time  $t$  and the parameters  $a = k_n^{-1}$  (reciprocal rate constant of nucleation),  $b$  (a constant related to nucleation),  $k_g$  (rate constant of crystal growth) and  $n$ , which represents the dimensionality of the crystal growth.<sup>12</sup> To find the right value for  $n$ , all dimensionalities were tested and the best fit,  $n = 3$  for CAU-18 and  $n = 1$  for CAU-19-H was found, which was substantiated by the SEM measurements (Fig. S13-14). The results of the Gualtieri fits for the reaction at 120 °C for both compounds are shown in Figure 13 and the resulting parameters are listed in Table 4. The Gualtieri fits for the



data obtained at the other reaction temperatures are shown in Figure S49 –S54. The rate constants for nucleation and crystal growth increase with temperature and can be used to calculate the probability of nucleation  $P_n$  which is given in eqn (2).

$$P_n = e^{-\frac{(t-a)^2}{b^2}} \quad (2)$$

$P_n$  is plotted versus time and depends on the Gualtieri constants  $a$  and  $b$ . The maximum of the probability of nucleation is shifted to smaller reaction times with increasing temperature (Fig. 12 and Table 4). The Arrhenius activation energy for nucleation and crystal growth can be obtained by plotting  $\ln(k)$  vs.  $1/T$  (Fig. S55 – S58). The Arrhenius activation energies were determined as 56(1) and 56(3)  $\text{kJ mol}^{-1}$  for nucleation and 48(1) and 58(5)  $\text{kJ mol}^{-1}$  for crystal growth for CAU-18 and CAU-19-H, respectively. The activation energies are in the same order of magnitude and in good agreement with other previous reported MOFs (Mn-MIL-100: 89.9/126.5  $\text{kJ mol}^{-1}$  (reference 9), MOF-14: 64-83  $\text{kJ mol}^{-1}$  (reference 10) CAU-13: 76-77  $\text{kJ mol}^{-1}$  (reference 69) and CAU-1: 131-136  $\text{kJ mol}^{-1}$  (reference 11)).

**Table 4.** Rate constants for nucleation ( $k_n$ ) and crystal growth ( $k_g$ ), nucleation parameter  $b$ , induction time ( $t_{ind}$ ), time to reach reaction completeness ( $t_{com}$ ) and maximum of probability of nucleation ( $P_n$ ) as obtained using the method of Gualtieri.<sup>12</sup> Values in brackets represent the reduced values  $t_{ind}$  and  $t_{com}$  for injection of the metal salt solution after 3 min to initiate the formation of CAU-19-H.

	$a=k_n^{-1}$	$k_g$	$b$	$t_{ind}$ [min]	$t_{com}$ [min]	$P_n$ (max.) [min]
CAU-18 110°C	16.43	0.09	5.43	9.7	37.0	16.3

<b>CAU-18 120 °C</b>	10.70	0.13	3.50	6.7	28.3	10.7
<b>CAU-18 130 °C</b>	6.89	0.19	1.86	5.0	17.7	7.0
<b>CAU-19-H 120 °C</b>	19.58	0.08	1.11	16.0 (13.0)	34.3 (31.3)	19.7
<b>CAU-19-H 130 °C</b>	12.36	0.13	0.63	9.7 (6.7)	22.3 (19.3)	12.3
<b>CAU-19-H 140 °C</b>	8.50	0.19	0.35	6.3 (3.3)	17.7 (14.7)	8.5

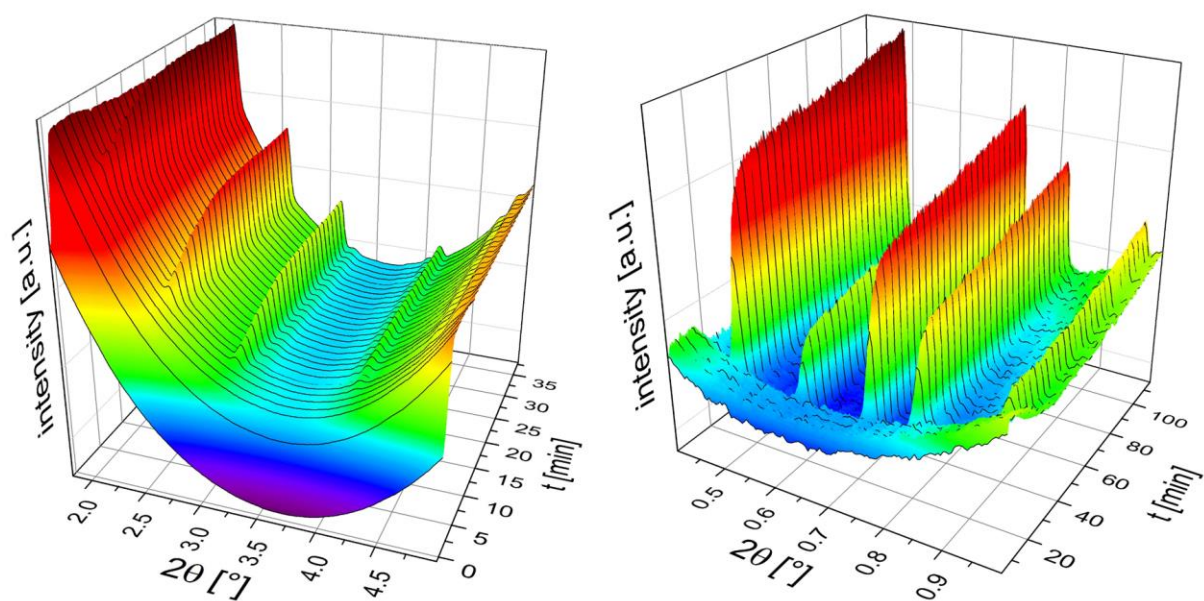


**Figure 11.** Results of the *in situ* XRD crystallization of CAU-18 (left) and CAU-19-H (right) at a reaction temperature of 120 °C. Measurements were carried out at beamlines P09 and P07B, PETRA III, DESY, Hamburg.

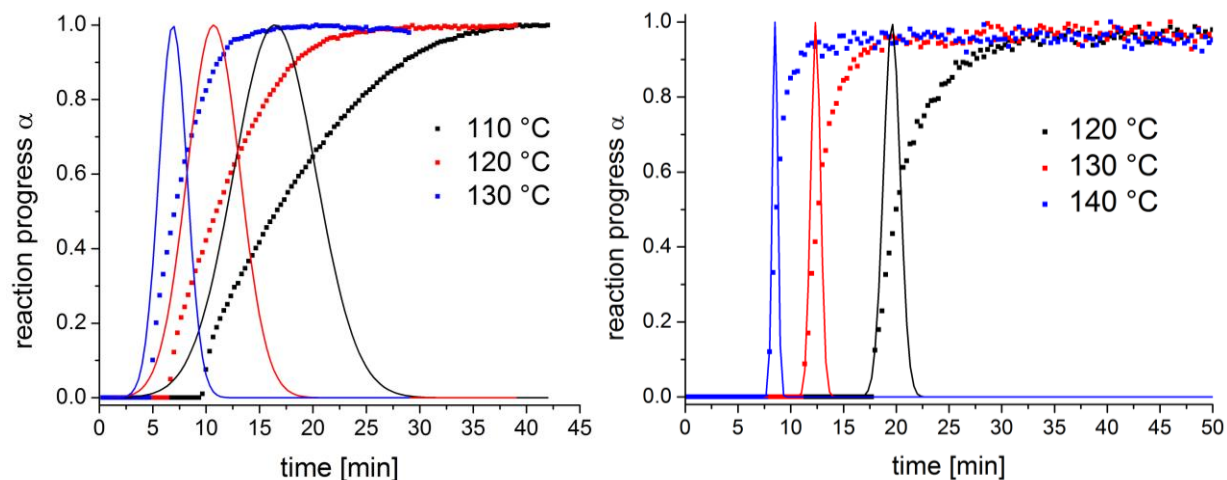


**Figure 12.** Reaction progress  $\alpha$  (filled squares) and probability of nucleation  $P_n$  (line) of CAU-18 (left) and CAU-19-H (right) as determined at the different reaction temperatures.

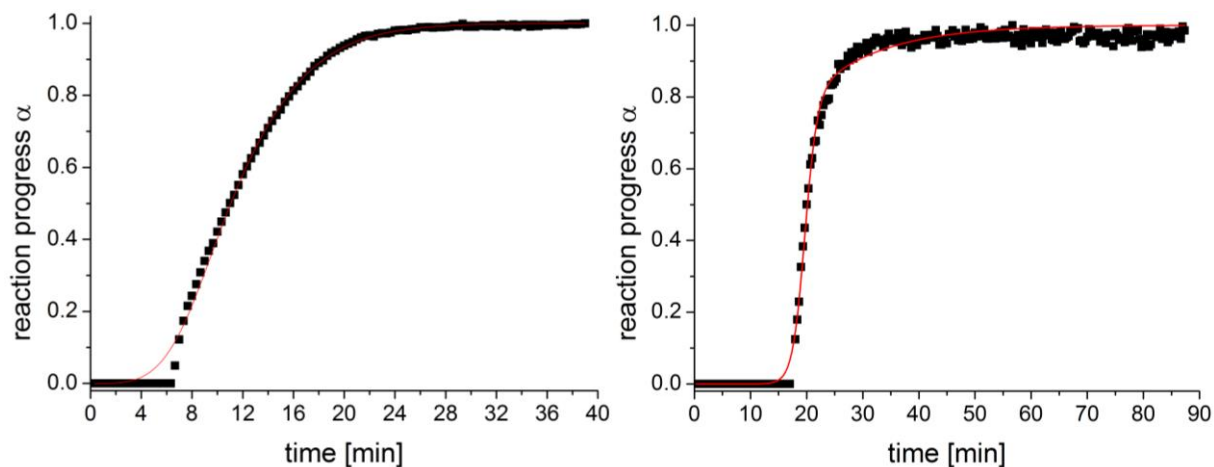


**Figure 13.** Gualtieri-fit of the reaction progress for the reactions carried out at 120 °C. Left, formation of CAU-18 and right, formation of CAU-19-H. The results of the fits are summarized in Figure S50 and S52.

**Conclusion.** We demonstrated the successful synthesis and characterization of four new porphyrin based Ce-MOFs, CAU-18,  $[\text{Ce}_4(\text{H}_2\text{TCPP})_3(\text{DMF})_2(\text{H}_2\text{O})_4]$ , CAU-18a,  $[\text{Ce}_4(\text{H}_2\text{TCPP})_3] \cdot 22 \text{ H}_2\text{O}$ , CAU-19-X,  $\text{Ce}_3(\text{H}_2\text{TCPP})_2(\text{BA-X})(\text{HBA-X/H}_2\text{O})_2] \cdot 2 \text{ HBA} \cdot x\text{H}_2\text{O}$  (X=H, 2Cl, 3Cl, 4Cl, 3CO<sub>2</sub>H, 4NH<sub>2</sub>, 4NO<sub>2</sub>) and Ce-PMOF-4NO<sub>2</sub>,  $[\text{Ce}_2(\text{H}_2\text{TCPP})(\text{C}_7\text{H}_4\text{O}_2\text{NO}_2)_2] \cdot 2 \text{ DMF}$  (H<sub>6</sub>TCPP = 4-tetracarboxyphenylporphyrin).

Considering this observed structural diversity induced by the presence/nature of the co-ligand employed, it could be very interesting to evaluate the other lanthanide ions in a similar manner. Furthermore the metalated form of CAU-19-H, M-CAU-19-H with M = Zn and Co, were obtained. Despite the use of (NH<sub>4</sub>)<sub>2</sub>[Ce(NO<sub>3</sub>)<sub>6</sub>] as a source of Ce in all syntheses, all compounds contain exclusively Ce<sup>3+</sup> ions. The trivalent oxidation state was unequivocally confirmed by XANES measurements. Thermal treatment of CAU-18 at 250 °C leads to the removal of DMF molecules and the permanently porous compound CAU-18a formed. Phase transformation of Ce-PMOF-NO<sub>2</sub> to CAU-19-NO<sub>2</sub> is observed in organic solvents at 70 °C within 72 h. CAU-18a and all CAU-19-X derivatives are permanently porous with specific surface areas of 330 - 600 m<sup>2</sup> g<sup>-1</sup> as determined from N<sub>2</sub> physisorption measurements at 77 K, and they are also porous towards H<sub>2</sub>O with an uptake between 10.7 and 21.3 wt%. The *in situ* crystallization studies revealed the expected temperature dependent increase of the rate constants for the formation of CAU-18 and CAU-19-H.

In this context it could be very interesting to further investigate the formation of the title compounds by *in-situ* XAS or EXAFS studies to gain insight into the reduction of the metal source and the relevance for the formation of Ce<sup>3+</sup>/Ce<sup>4+</sup> MOFs.

## ASSOCIATED CONTENT

### **Supporting Information.**

Details of the synthesis and characterization of H<sub>6</sub>TCPP, Co-H<sub>4</sub>TCPP and information on the characterization of all obtained compounds, including <sup>1</sup>H-NMR spectroscopy, Pawley-fits, XANES spectra, structural representations, thermogravimetric measurements and IR-spectroscopy. CCDC 1539771-1539772 contains the supplementary crystallographic data for this paper. These data can be obtained free of charge from The Cambridge Crystallographic Data Centre via [www.ccdc.cam.ac.uk/getstructures](http://www.ccdc.cam.ac.uk/getstructures).

## AUTHOR INFORMATION

### **Corresponding Author**

\* [stock@ac.uni-kiel.de](mailto:stock@ac.uni-kiel.de) (N.S.)

## ACKNOWLEDGEMENT

We appreciate support from the Deutsche Forschungsgemeinschaft (SPP-1415; STO 643/6-2). We would like to acknowledge Milan Köppen for the development of software tools used for data treatment and DESY for the allocation of beamtime. Furthermore we thank Jörg Stremper and the beamline staff of beamline P07 and P09 for their support during the beamtime as well as HZG and Norbert Schell. This work has been supported by the MATsynCELL project through the Röntgen-Ångström Cluster, supported by the Swedish Research Council and the German Federal Ministry of Education and Research (BMBF). K.A.L. and A.V.S. acknowledge the Mega-grant of the Russian Federation Government no. 14.Y26.31.0001. K.A.L. acknowledges

the support from the Russian Foundation for Basic Research, project no. 16-32-00572 мол\_a. Furthermore we thank Simon Smolders from the KU Leuven for measuring the TG curves of Zn- and Co-CAU-19-H Figures S40 and S41.

## References

- (1) Furukawa, H.; Cordova, K. E.; O’Keeffe, M.; Yaghi, O. M. The Chemistry and Applications of Metal-Organic Frameworks. *Science* **2013**, *341*.
- (2) Stock, N.; Reinsch, H.; Schilling, L.-H. CHAPTER 2 Synthesis of MOFs. *Metal Organic Frameworks as Heterogeneous Catalysts*; The Royal Society of Chemistry, 2013; pp 9–30.
- (3) Zhou, H.-C.; Long, J. R.; Yaghi, O. M. Introduction to Metal–Organic Frameworks. *Chem Rev* **2012**, *112*, 673–674.
- (4) Yaghi, O. M.; O’Keeffe, M.; Ockwig, N. W.; Chae, H. K.; Eddaoudi, M.; Kim, J. Reticular synthesis and the design of new materials. *Nature* **2003**, *423*, 705–714.
- (5) Sun, C.-Y.; Qin, C.; Wang, X.-L.; Su, Z.-M. Metal-organic frameworks as potential drug delivery systems. *Expert Opinion on Drug Delivery* **2013**, *10*, 89–101.
- (6) Janiak, C.; Vieth, J. K. MOFs, MILs and more: concepts, properties and applications for porous coordination networks (PCNs). *New J Chem* **2010**, *34*, 2366–2388.
- (7) Mueller, U.; Schubert, M.; Teich, F.; Puetter, H.; Schierle-Arndt, K.; Pastre, J. Metal-organic frameworks-prospective industrial applications. *J Mater Chem* **2006**, *16*, 626–636.
- (8) Millange, F.; Medina, M. I.; Guillou, N.; Férey, G.; Golden, K. M.; Walton, R. I. Time-Resolved In Situ Diffraction Study of the Solvothermal Crystallization of Some Prototypical Metal–Organic Frameworks. *Angew Chem, Int Ed Engl* **2010**, *49*, 763–766.
- (9) Reinsch, H.; Stock, N. Formation and characterisation of Mn-MIL-100. *CrystEngComm* **2013**, *15*, 544–550.
- (10) Millange, F.; El Osta, R.; Medina, M. E.; Walton, R. I. A time-resolved diffraction study of a window of stability in the synthesis of a copper carboxylate metal-organic framework. *CrystEngComm* **2011**, *13*, 103–108.
- (11) Ahnfeldt, T.; Moellmer, J.; Guillerm, V.; Staudt, R.; Serre, C.; Stock, N. High-Throughput and Time-Resolved Energy-Dispersive X-Ray Diffraction (EDXRD) Study of the Formation of CAU-1-(OH)2: Microwave and Conventional Heating. *Chem--Eur J* **2011**, *17*, 6462–6468.
- (12) Gualtieri, F. A. Synthesis of sodium zeolites from a natural halloysite. *Phys Chem Miner* **2001**, *28*, 719–728.
- (13) Feng, D.; Jiang, H.-L.; Chen, Y.-P.; Gu, Z.-Y.; Wei, Z.; Zhou, H.-C. Metal–Organic Frameworks Based on Previously Unknown Zr8/Hf8 Cubic Clusters. *Inorg Chem* **2013**, *52*, 12661–12667.
- (14) Feng, D.; Chung, W.-C.; Wei, Z.; Gu, Z.-Y.; Jiang, H.-L.; Chen, Y.-P.; Darensbourg, D. J.; Zhou, H.-C. Construction of Ultrastable Porphyrin Zr Metal–Organic Frameworks through Linker Elimination. *J Am Chem Soc* **2013**, *135*, 17105–17110.
- (15) Gallagher, A. T.; Kelty, M. L.; Park, J. G.; Anderson, J. S.; Mason, J. A.; Walsh, J. P. S.; Collins, S. L.; Harris, T. D. Dioxygen binding at a four-coordinate cobaltous porphyrin site in a metal-organic framework: structural, EPR, and O2 adsorption analysis. *Inorg Chem Front* **2016**, *3*, 536–540.

- (16) Hod, I.; Sampson, M. D.; Deria, P.; Kubiak, C. P.; Farha, O. K.; Hupp, J. T. Fe-Porphyrin-Based Metal–Organic Framework Films as High-Surface Concentration, Heterogeneous Catalysts for Electrochemical Reduction of CO<sub>2</sub>. *ACS Catalysis* **2015**, *5*, 6302–6309.
- (17) Chang, T.-H.; Kung, C.-W.; Chen, H.-W.; Huang, T.-Y.; Kao, S.-Y.; Lu, H.-C.; Lee, M.-H.; Boopathi, K. M.; Chu, C.-W.; Ho, K.-C. Planar Heterojunction Perovskite Solar Cells Incorporating Metal–Organic Framework Nanocrystals. *Adv Mater (Weinheim, Ger)* **2015**, *27*, 7229–7235.
- (18) Kung, C.-W.; Chang, T.-H.; Chou, L.-Y.; Hupp, J. T.; Farha, O. K.; Ho, K.-C. Post metalation of solvothermally grown electroactive porphyrin metal-organic framework thin films. *Chem Commun* **2015**, *51*, 2414–2417.
- (19) Liu, Y.; Howarth, A. J.; Hupp, J. T.; Farha, O. K. Selective Photooxidation of a Mustard-Gas Simulant Catalyzed by a Porphyrinic Metal–Organic Framework. *Angew Chem, Int Ed Engl* **2015**, *54*, 9001–9005.
- (20) Guo, Z.; Chen, B. Recent developments in metal-metalloporphyrin frameworks. *Dalton Trans* **2015**, *44*, 14574–14583.
- (21) Lammert, M.; Wharmby, M. T.; Smolders, S.; Bueken, B.; Lieb, A.; Lomachenko, K. A.; Vos, D. D.; Stock, N. Cerium-based metal organic frameworks with UiO-66 architecture: synthesis, properties and redox catalytic activity. *Chem Commun* **2015**, *51*, 12578–12581.
- (22) Alves, E.; Faustino, M. A. F.; Neves, Maria G. P. M. S.; Cunha, Â.; Nadais, H.; Almeida, A. Potential applications of porphyrins in photodynamic inactivation beyond the medical scope. *J Photochem Photobiol, C* **2015**, *22*, 34–57.
- (23) Huang, H.; Song, W.; Rieffel, J.; Lovell, J. F. Emerging Applications of Porphyrins in Photomedicine. *Front. in Phys.* **2015**, *3*.
- (24) Lu, K.; He, C.; Lin, W. A Chlorin-Based Nanoscale Metal–Organic Framework for Photodynamic Therapy of Colon Cancers. *J Am Chem Soc* **2015**, *137*, 7600–7603.
- (25) Devic, T.; Serre, C. High valence 3p and transition metal based MOFs. *Chem Soc Rev* **2014**, *43*, 6097–6115.
- (26) Gao, W.-Y.; Chrzanowski, M.; Ma, S. Metal-metalloporphyrin frameworks: a resurging class of functional materials. *Chem Soc Rev* **2014**, *43*, 5841–5866.
- (27) Guo, Z.; Chen, B. Recent developments in metal-metalloporphyrin frameworks. *Dalton Trans* **2015**, *44*, 14574–14583.
- (28) Huh, S.; Kim, S.-J.; Kim, Y. Porphyrinic metal-organic frameworks from custom-designed porphyrins. *CrystEngComm* **2016**.
- (29) Kosal, M. E.; Chou, J.-H.; Wilson, S. R.; Suslick, K. S. A functional zeolite analogue assembled from metalloporphyrins. *Nat Mater* **2002**, *1*, 118–121.
- (30) Goldberg, I. Metalloporphyrin Molecular Sieves. *Chem--Eur J* **2000**, *6*, 3863–3870.
- (31) Feng, D.; Gu, Z.-Y.; Chen, Y.-P.; Park, J.; Wei, Z.; Sun, Y.; Bosch, M.; Yuan, S.; Zhou, H.-C. A Highly Stable Porphyrinic Zirconium Metal–Organic Framework with shp-a Topology. *J Am Chem Soc* **2014**, *136*, 17714–17717.
- (32) Jiang, H.-L.; Feng, D.; Wang, K.; Gu, Z.-Y.; Wei, Z.; Chen, Y.-P.; Zhou, H.-C. An Exceptionally Stable, Porphyrinic Zr Metal–Organic Framework Exhibiting pH-Dependent Fluorescence. *J Am Chem Soc* **2013**, *135*, 13934–13938.
- (33) Morris, W.; Voloskiy, B.; Demir, S.; Gándara, F.; McGrier, P. L.; Furukawa, H.; Cascio, D.; Stoddart, J. F.; Yaghi, O. M. Synthesis, Structure, and Metalation of Two New Highly Porous Zirconium Metal–Organic Frameworks. *Inorg Chem* **2012**, *51*, 6443–6445.

- (34) Bai, Y.; Dou, Y.; Xie, L.-H.; Rutledge, W.; Li, J.-R.; Zhou, H.-C. Zr-based metal-organic frameworks: design, synthesis, structure, and applications. *Chem Soc Rev* **2016**, *45*, 2327–2367.
- (35) Feng, D.; Jiang, H.-L.; Chen, Y.-P.; Gu, Z.-Y.; Wei, Z.; Zhou, H.-C. Metal–Organic Frameworks Based on Previously Unknown Zr<sub>8</sub>/Hf<sub>8</sub> Cubic Clusters. *Inorg Chem* **2013**, *52*, 12661–12667.
- (36) Fateeva, A.; Chater, P. A.; Ireland, C. P.; Tahir, A. A.; Khimyak, Y. Z.; Wiper, P. V.; Darwent, J. R.; Rosseinsky, M. J. A Water-Stable Porphyrin-Based Metal–Organic Framework Active for Visible-Light Photocatalysis. *Angew Chem* **2012**, *124*, 7558–7562.
- (37) Rhauderwiek, T.; Waitschat, S.; Wuttke, S.; Reinsch, H.; Bein, T.; Stock, N. Nanoscale Synthesis of Two Porphyrin-Based MOFs with Gallium and Indium. *Inorg Chem* **2016**, *55*, 5312–5319.
- (38) Gao, W.-Y.; Zhang, Z.; Cash, L.; Wojtas, L.; Chen, Y.-S.; Ma, S. Two rare indium-based porous metal-metalloporphyrin frameworks exhibiting interesting CO<sub>2</sub> uptake. *CrystEngComm* **2013**, *15*, 9320–9323.
- (39) Johnson, J. A.; Luo, J.; Zhang, X.; Chen, Y.-S.; Morton, M. D.; Echeverría, E.; Torres, F. E.; Zhang, J. Porphyrin-Metalation-Mediated Tuning of Photoredox Catalytic Properties in Metal–Organic Frameworks. *ACS Catalysis* **2015**, *5*, 5283–5291.
- (40) Johnson, J. A.; Zhang, X.; Reeson, T. C.; Chen, Y.-S.; Zhang, J. Facile Control of the Charge Density and Photocatalytic Activity of an Anionic Indium Porphyrin Framework via in Situ Metalation. *J Am Chem Soc* **2014**, *136*, 15881–15884.
- (41) Fateeva, A.; Devautour-Vinot, S.; Heymans, N.; Devic, T.; Grenèche, J.-M.; Wuttke, S.; Miller, S.; Lago, A.; Serre, C.; Weireld, G. de *et al.* Series of Porous 3-D Coordination Polymers Based on Iron(III) and Porphyrin Derivatives. *Chem Mater* **2011**, *23*, 4641–4651.
- (42) Fateeva, A.; Clarisse, J.; Pilet, G.; Grenèche, J.-M.; Nouar, F.; Abeykoon, B. K.; Guegan, F.; Goutaudier, C.; Luneau, D.; Warren, J. E. *et al.* Iron and Porphyrin Metal–Organic Frameworks: Insight into Structural Diversity, Stability, and Porosity. *Cryst Growth Des* **2015**, *15*, 1819–1826.
- (43) Wang, K.; Feng, D.; Liu, T.-F.; Su, J.; Yuan, S.; Chen, Y.-P.; Bosch, M.; Zou, X.; Zhou, H.-C. A Series of Highly Stable Mesoporous Metalloporphyrin Fe-MOFs. *J Am Chem Soc* **2014**, *136*, 13983–13986.
- (44) Yang, F.; Jing, L.; Ji, L.; Liu, Q.; Zhang, X. Design, fabrication and the relative catalytic properties of metal-organic framework complexes based on tetra(4-carboxyphenyl)porphyrin and cerium ions. *CrystEngComm* **2014**, *16*, 4274–4280.
- (45) Lipstman, S.; Goldberg, I. 2D and 3D coordination networks of tetra(carboxyphenyl)-porphyrins with cerium and thulium ions. *J Mol Struct* **2008**, *890*, 101–106.
- (46) Muniappan, S.; Lipstman, S.; George, S.; Goldberg, I. Porphyrin Framework Solids. Synthesis and Structure of Hybrid Coordination Polymers of Tetra(carboxyphenyl)porphyrins and Lanthanide-Bridging Ions. *Inorg Chem* **2007**, *46*, 5544–5554.
- (47) Lipstman, S.; Muniappan, S.; George, S.; Goldberg, I. Framework coordination polymers of tetra(4-carboxyphenyl)porphyrin and lanthanide ions in crystalline solids. *Dalton Trans* **2007**, 3273–3281.
- (48) Jeong, E.-Y.; Ansari, M. B.; Mo, Y.-H.; Park, S.-E. Removal of Cu(II) from water by tetrakis(4-carboxyphenyl) porphyrin-functionalized mesoporous silica. *J Hazard Mater* **2011**, *185*, 1311–1317.
- (49) Harada, A.; Yamaguchi, H.; Okamoto, K.; Fukushima, H.; Shiotsuki, K.; Kamachi, M. Control of Photoinduced Electron Transfer from Zinc-Porphyrin to Methyl Viologen by



Supramolecular Formation between Monoclonal Antibody and Zinc-Porphyrin. *Photochem Photobiol* **1999**, *70*, 298–302.

(50) Garcia, G.; Sol, V.; Lamarche, F.; Granet, R.; Guilloton, M.; Champavier, Y.; Krausz, P. Synthesis and photocytotoxic activity of new chlorin–polyamine conjugates. *Bioorg Med Chem Lett* **2006**, *16*, 3188–3192.

(51) Chen, W.; Fukuzumi, S. Change in Supramolecular Networks through In Situ Esterification of Porphyrins. *Eur J Inorg Chem* **2009**, *2009*, 5494–5505.

(52) Feng, D.; Gu, Z.-Y.; Li, J.-R.; Jiang, H.-L.; Wei, Z.; Zhou, H.-C. Zirconium-Metalloporphyrin PCN-222: Mesoporous Metal–Organic Frameworks with Ultrahigh Stability as Biomimetic Catalysts. *Angew Chem* **2012**, *124*, 10453–10456.

(53) Bruker. *SAINT V9.32B*, Bruker AXS Inc; Madison, Wisconsin, USA, 2012.

(54) Sheldrick, G. A short history of SHELX. *Acta Crystallogr, Sect A: Found Crystallogr* **2008**, *64*, 112–122.

(55) Dolomanov, O. V.; Bourhis, L. J.; Gildea, R. J.; Howard, J. A. K.; Puschmann, H. OLEX2: a complete structure solution, refinement and analysis program. *J Appl Crystallogr* **2009**, *42*, 339–341.

(56) Klementiev, K.; Chernikov, R. XAFSmass: a program for calculating the optimal mass of XAFS samples. *J. of Phys.: Conf. Ser.* **2016**, *712*, 12008.

(57) Coelho, A. *TOPAS-Academic V4.1*; Coelho Software, 2007.

(58) Brandenburg, K. *Diamond Version 3*; Crystal Impact GbR: Bonn, 2012.

(59) Strempler, J.; Francoual, S.; Reuther, D.; Shukla, D. K.; Skaugen, A.; Schulte-Schrepping, H.; Kracht, T.; Franz, H. Resonant scattering and diffraction beamline P09 at PETRA III. *Journal of Synchrotron Radiation* **2013**, *20*, 541–549.

(60) H.G. Brokmeier, M. Müller, P.K. Pranzas, A. Schreyer and P. Staron. The High Energy Materials Science Beamline (HEMS) at PETRA III. *Mater Sci Forum* **2014**, *772*, 57–61.

(61) Heidenreich, N.; Rütt, U.; Köppen, M.; Inge, A. K.; Beier, S.; Dippel, A.-C.; Suren, R.; Stock, N. A multi-purpose reaction cell for the investigation of reactions under solvothermal conditions. *Rev. Sci. Instrum.* **2017**, *submitted*.

(62) Afzal, S.; Daoud, W. A.; Langford, S. J. Self-cleaning cotton by porphyrin-sensitized visible-light photocatalysis. *J Mater Chem* **2012**, *22*, 4083–4088.

(63) Rochford, J.; Chu, D.; Hagfeldt, A.; Galoppini, E. Tetrachelate Porphyrin Chromophores for Metal Oxide Semiconductor Sensitization: Effect of the Spacer Length and Anchoring Group Position. *J Am Chem Soc* **2007**, *129*, 4655–4665.

(64) Coxall, R. A.; Harris, S. G.; Henderson, D. K.; Parsons, S.; Tasker, P. A.; Winpenny, R. E. P. Inter-ligand reactions: in situ formation of new polydentate ligands. *J Chem Soc, Dalton Trans* **2000**, 2349–2356.

(65) Han, Y.; Li, X.; Li, L.; Ma, C.; Shen, Z.; Song, Y.; You, X. Structures and Properties of Porous Coordination Polymers Based on Lanthanide Carboxylate Building Units. *Inorg Chem* **2010**, *49*, 10781–10787.

(66) J. Rouquerol; D. Avnir; C. W. Fairbridge; D. H. Everett; J. M. Haynes; N. Pernicone; J. D. F. Ramsay; K. S. W. Sing; Unger, K. K. Recommendations for the characterization of porous solids (Technical Report). *pac* **1994**, *66*, 1739–1758.

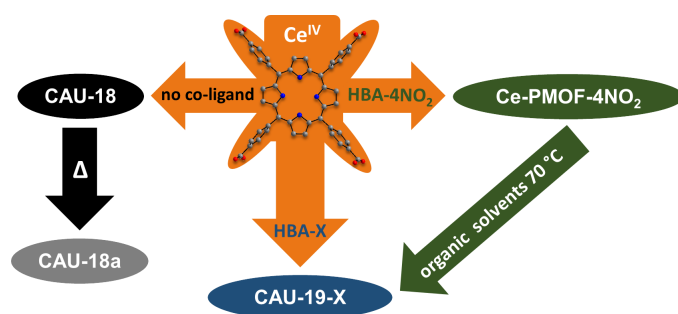
(67) Thommes, M.; Kaneko, K.; Neimark Alexander, V.; Olivier James, P.; Rodriguez-Reinoso, F.; Rouquerol, J.; Sing Kenneth, S. W. Physisorption of gases, with special reference to the evaluation of surface area and pore size distribution (IUPAC Technical Report). *pac* **2015**, *0*.

- (68) Pienack, N.; Bensch, W. In-Situ Monitoring of the Formation of Crystalline Solids. *Angew Chem, Int Ed Engl* **2011**, *50*, 2014–2034.
- (69) Niekel, F.; Ackermann, M.; Guerrier, P.; Rothkirch, A.; Stock, N. Aluminum-1,4-cyclohexanedicarboxylates: High-Throughput and Temperature-Dependent in Situ EDXRD Studies. *Inorg Chem* **2013**, *52*, 8699–8705.
- (70) Antonova, E.; Seidlhofer, B.; Wang, J.; Hinz, M.; Bensch, W. Controlling Nucleation and Crystal Growth of a Distinct Polyoxovanadate Cluster: An In Situ Energy Dispersive X-ray Diffraction Study under Solvothermal Conditions. *Chem--Eur J* **2012**, *18*, 15316–15322.
- (71) Seidlhofer, B.; Antonova, E.; Wang, J.; Schinkel, D.; Bensch, W. On the Complexity of Crystallization of Thioantimonates: In-situ Energy Dispersive X-ray Diffraction (EDXRD) Studies of the Solvothermal Formation of the Isostructural Thioantimonates [TM(tren)Sb<sub>4</sub>S<sub>7</sub>] (TM = Fe, Zn). *Z Anorg Allg Chem* **2012**, *638*, 2555–2564.

## For Table of Content Use Only

### Co-ligand dependent Formation and Phase Transformation of Four Porphyrin-based Cerium MOFs

*Timo Rhauderwiek, Niclas Heidenreich, Helge Reinsch, Sigurd Øien-Ødegaard, Kirill A. Lomachenko, Uta Rütt, Alexander V. Soldatov, Karl Petter Lillerud, Norbert Stock*



Four porphyrin-based Ce(III)-MOFs were synthesized starting from a Ce(IV) source. CAU-18/CAU-19-X (X = various functional groups) are formed in the absence/presence of a benzoic acid derivative HBA-X. Phase transformation of the as-synthesized compounds CAU-18 and Ce-PMOF-4NO<sub>2</sub> was observed upon thermal treatment. The formation of CAU-18 and CAU-19-X was also investigated by *in situ* PXRD studies using synchrotron radiation.